nature neuroscience

Article

https://doi.org/10.1038/s41593-024-01681-9

Control and recalibration of path integration in place cells using optic flow

Received: 28 June 2022

Accepted: 13 May 2024

Published online: 27 June 2024

Check for updates

Manu S. Madhav[1,2,3,4,5,9] ✉, Ravikrishnan P. Jayakumar[1,3,6,9], Brian Y. Li[1], Shahin G. Lashkari[3,6], Kelly Wright[1], Francesco Savelli[1,8], James J. Knierim[1,2,7,10] ✉ & Noah J. Cowan[3,6,10] ✉

Hippocampal place cells are influenced by both self-motion (idiothetic) signals and external sensory landmarks as an animal navigates its environment. To continuously update a position signal on an internal 'cognitive map', the hippocampal system integrates self-motion signals over time, a process that relies on a finely calibrated path integration gain that relates movement in physical space to movement on the cognitive map. It is unclear whether idiothetic cues alone, such as optic flow, exert sufficient influence on the cognitive map to enable recalibration of path integration, or if polarizing position information provided by landmarks is essential for this recalibration. Here, we demonstrate both recalibration of path integration gain and systematic control of place fields by pure optic flow information in freely moving rats. These findings demonstrate that the brain continuously rebalances the influence of conflicting idiothetic cues to fine-tune the neural dynamics of path integration, and that this recalibration process does not require a top-down, unambiguous position signal from landmarks.

The spatial firing fields of hippocampal place cells are determined by allothetic inputs (such as visual landmarks and environmental boundaries) and path integration of idiothetic inputs (such as optic flow and vestibular signals)[1–9]. Decades of research have provided detailed insight into how allothetic cues can exert precise control over the firing of place cells[3,6,7,10–13]. However, much less is understood about the mechanisms by which idiothetic cues affect place cells because, in the absence of landmarks, the updating of the map by path integration[14,15] is unstable—when only idiothetic cues are available, the internal representation drifts and rapidly becomes unbound to the world frame of refs. 1,2,15,16.

Control theory provides a basis for stabilizing unstable systems and thus provides a powerful experimental arsenal to disentangle the elements of neural computation[17–22]. Famously, the voltage clamp allowed Hodgkin and Huxley to stabilize the membrane potential at a constant reference to pinpoint the roles of individual ion channels[23]. More recently, a growing body of literature has garnered new insights into neural computation by using control engineering to close feedback loops on neural representations[24–27]. Here, we extend the application of control theory in biology[18,28] to high-order spatial representations; specifically, we introduce a controller that uses neural feedback to implement a 'cognitive clamp', maintaining at a desired reference an essential cognitive variable for forming the hippocampal cognitive map, the gain of the path integrator[29–31]. This gain relates self-motion information from idiothetic cues to an updating of position on the internal hippocampal representation and must be fine-tuned with experience (that is, recalibrated) based on an animal's sensorimotor experience to ensure accurate path integration[6,7,31].

[1]Mind/Brain Institute, Johns Hopkins University, Baltimore, MD, USA. [2]Kavli Neuroscience Discovery Institute, Johns Hopkins University, Baltimore, MD, USA. [3]Laboratory for Computational Sensing and Robotics, Johns Hopkins University, Baltimore, MD, USA. [4]School of Biomedical Engineering, University of British Columbia, Vancouver, British Columbia, Canada. [5]Djavad Mowafaghian Centre for Brain Health, University of British Columbia, Vancouver, British Columbia, Canada. [6]Mechanical Engineering Department, Johns Hopkins University, Baltimore, MD, USA. [7]Solomon H. Snyder Department of Neuroscience, Johns Hopkins University, Baltimore, MD, USA. [8]Present address: Department of Neuroscience, Developmental and Regenerative Biology, The University of Texas at San Antonio, San Antonio, TX, USA. [9]These authors contributed equally: Manu S. Madhav, Ravikrishnan P. Jayakumar. [10]These authors jointly supervised this work: James J. Knierim, Noah J. Cowan. ✉e-mail: manu.madhav@ubc.ca; jknierim@jhu.edu; ncowan@jhu.edu

https://doi.org/10.1038/s41593-024-01681-9

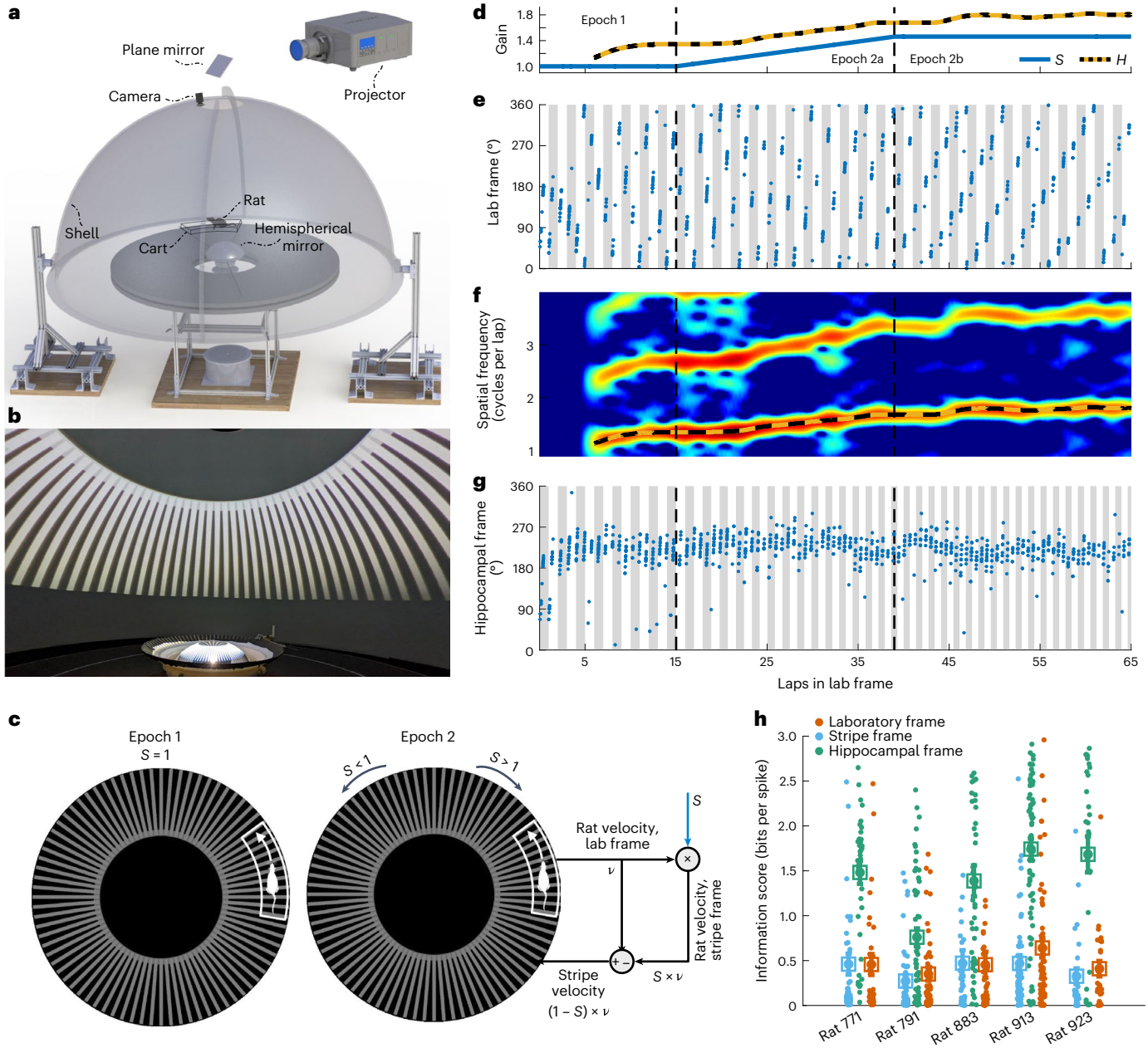

Fig. 1 | Stripe presentation and gain computation. a, Virtual reality Dome apparatus (reproduced from ref. 32). Rats ran on a circular table surrounded by a hemispherical shell. A projector image reflects off a hemispherical mirror onto the inner surface of the shell. **b**, Stripes projected within the dome. **c**, Stripe gain, S, related the velocity of the rat with respect to the lab and stripe frames. In Epoch 1, stripes were stationary ($S = 1$). In Epoch 2, stripes were moved in the same ($S < 1$) or opposite ($S > 1$) direction of the rat: the stripe velocity $(1 - S)v$ was the difference between velocity of the rat in the lab and stripe frames. **d**–**g**, Hippocampal gain decoding. The x axis shows the number of laps the rat ran on the table. **d**, Stripe gain (S; blue) and hippocampal gain (H; dashed yellow) during Epochs 1 and 2 in one session. $S = 1$ in Epoch 1 and was ramped up to and held at $S = 1.46$ during Epoch 2. H begins only at lap 6 because of the six-lap window used to estimate H. **e**, Spikes from one unit (blue) plotted as a function of the rat's angle θ (°) relative to the lab. Gray/white vertical bars denote laps in the lab frame. The unit fired at the same location in the lab frame ($H \simeq 1$) for the first two laps but its place field began to drift backward starting at lap 3 ($H > 1$). **f**, Spatial spectrogram of firing rate of this unit; the y axis denotes spatial frequency and color denotes power. The dominant spatial frequency H (dashed line) and its second harmonic are evident. **g**, Same spikes as **e** plotted in the hippocampal frame ($Y = \int H \, d\theta$, wrapped at 360°); gray/white bars are laps in this frame. Firing fields aligned in the hippocampal frame indicate accurate decoding of H. **h**, Spatial information scores in the hippocampal frame are significantly higher than those in laboratory and stripe frames for each rat (one-sided Wilcoxon signed rank tests on mean information across rats: hippocampus versus laboratory, rank = 15.0, $P = 0.031$; hippocampus versus stripes, rank = 15.0, $P = 0.031$; stripes versus laboratory, rank = 2, $P = 0.94$). To avoid counting the same cell multiple times, for each rat only the session with the greatest number of units ($n = 43, 64, 49, 78, 28$) was used in this analysis. Data are mean ± s.e.m. with scores from individual units shown.

To achieve this level of cognitive control, we used a unique, immersive planetarium-style virtual reality apparatus (the 'Dome'[32]; Fig. 1a) to provide pure optic flow input to a running rat while recording hippocampal place cells. In all sessions, the movements of the optic flow cues (stripes; Fig. 1b) along the azimuthal periphery of the Dome were tied to the movement of the rat such that the rat's velocity with respect to the stripes was directly controlled by a behavioral feedback loop modulating the velocity of the stripes (Fig. 1c). In addition to this behavioral feedback loop, our study consisted of two conditions related to the absence (open-loop) or presence (closed-loop) of a neural feedback

control loop. In open-loop experiments, a predetermined stripe gain profile controlled the stripe velocity, similar to previous behavioral[18,33–40] and neurophysiological[41–48] experiments in humans and other animals. In contrast, in neurally closed-loop experiments, the stripe gain was modulated as a function of the real-time place cell activity state with respect to a desired activity state. (The terms 'open-loop' and 'closed-loop' throughout this paper refer specifically to the absence or presence of this neurally closed feedback loop, as the behavioral feedback loop was always present.) This neural feedback stabilized the path integrator gain in the absence of an allothetic spatial reference frame that would typically be provided by landmarks. We found that optic flow cues, in the absence of an external, landmark-based reference frame, could exert reliable control over the hippocampal place cell map and could also induce a recalibration of the gain of the path integration system when the optic flow cues were placed in constant conflict with other idiothetic cues.

Results

Open-loop stripe manipulation influences hippocampal gain

Spatially alternating light and dark stripes were projected onto the inside of the Dome shell to provide a pure optic flow signal (Fig. 1b). Unlike in our previous study[6], there were no salient, polarizing landmarks in the Dome, and thus the rats were presumably forced to rely on idiothetic cues and path integration to maintain their internal estimate of location as they ran laps. The stripes were moved according to a gain S, which determined the ratio of the rat's speed relative to the stripes to the rat's speed in the lab frame (Fig. 1c). The stripes moved only when the rat moved. When $S > 1$, the stripes moved in the direction opposite to the rat's movement. When $S < 1$, the stripes moved in the same direction as the rat but at a lower speed. When $S = 1$, the stripes did not move at all. For example, if a rat ran counterclockwise (CCW), then with $S = 2$, the stripes moved clockwise (CW) at the same speed as the rat. Likewise, with $S = 0.5$, the stripes moved CCW at half the speed of the rat. Experimental sessions were segmented into epochs according to how the stripe gain was manipulated. During Epoch 1, rats ran CCW for 15 laps with $S = 1$ (stripes were stationary; Fig. 1d, Epoch 1). During Epoch 2, S diverged from 1 according to a predetermined profile (stripes were rotated; Fig. 1d, Epochs 2a and 2b), segmented into a linear rising or falling phase and a constant plateau for S (Epochs 2a and 2b, respectively; Fig. 1d).

Results of a typical open-loop session are shown in Fig. 1d–g ($n = 5$ rats, 40 sessions, mean 22 units per session (range 3–58 units) meeting place cell inclusion criteria; Methods). For the first 15 laps, place fields drifted backward each lap. This drift is a consequence of the error that accumulates every lap when the animal must rely solely on path integration without any landmarks to prevent and/or correct drift. Importantly, this drift indicates that any landmarks in the environment (inside or outside the Dome) were insufficient for the rat to anchor its map, validating our experimental strategy. On lap 16, we began to rotate the stripes by ramping the stripe gain S up to a value of 1.461. The place fields drifted more swiftly, in the same direction as the stripe movement. This increased drift indicates that optic flow alone can qualitatively influence place fields[44], similar to previous work with thalamic head direction cells in rats[43] and retrosplenial spatial cells in mice[42].

To quantify the drift of place fields over time, we estimated the gain of the hippocampus using an improved version of the population decoder used in our previous study[6]. The hippocampal gain H can be thought of as the relationship between the animal's physical movement through the world and the updating of its position on the cognitive map. When $H = 1$, the firing pattern of a spatial cell repeats precisely once per lap; when $H < 1$, in contrast, the pattern repeats less frequently than once per lap, that is, the rat's position on its hippocampal map updates more slowly than the rat's actual movement on the track (and vice versa when $H > 1$). The population decoder worked by first determining the gain of each active place cell based on the spatial periodicity of its firing rate (Fig. 1f) and then computing the median gain across the population of active place cells (Methods and Extended Data Fig. 1). The median operation filtered out small variations in lap-to-lap firing of individual cells. The gains estimated from individual place cells recorded in a given session were almost always tightly coherent with each other during the manipulations of optic flow (Fig. 2g,h). Putative pyramidal cells (1,549 units) and interneurons (85 units) were both coherent to the overall population (Extended Data Fig. 2), and thus were combined in all analyses of hippocampal gain. By integrating the decoded value of H, we computed the position of the rat in its own internal reference frame, which we term the hippocampal frame. The rate maps of place cells calculated in the hippocampal frame (Fig. 1g) had greater spatial information than rate maps calculated in either the laboratory frame or the moving-stripe frame, whereas results in laboratory and stripe frames were not significantly different from each other (Fig. 1h). These results indicated that the decoding of H produced stable, internally coherent rate maps in the hippocampal frame of reference.

Pure optic flow cues exerted demonstrable influence over the hippocampal representation in all five rats (Fig. 2a–f,i and Extended Data Fig. 3). Across sessions, we varied the stripe gain between 0.231 and 1.769 to produce a parametric description of how optic flow cues influenced the hippocampal spatial map. Figure 2a shows a control session when S was maintained at 1 (blue line) (that is, the stripes were stationary). The hippocampal gain H started out at approximately 1.13 in the first laps of Epoch 1, and this value gradually increased over the course of the session. Because $H > 1$, the place fields drifted backward on the track throughout the session (five place cells recorded simultaneously in Fig. 2b), and the rate of drift slightly increased (that is, the slopes of each cell's lap-by-lap field location became steeper with increasing laps). This backward drift ($H > 1$) was present in Epochs 1 and 2b in most sessions (Extended Data Fig. 4a,b), indicating that the system may be biased to overestimate the animal's distance traveled[49,50] in the absence of landmarks that provide an absolute reference frame. When plotted in the hippocampal frame (Fig. 2b, bottom), each cell's place field was stable, demonstrating that the hippocampal map drifted coherently. Figure 2c,d shows an example session where $S_{final} = 1.46$. Here, H settled to a relatively steady value of $H_{baseline} = 1.35$ in Epoch 1, and then began to rise sharply in Epoch 2a, paralleling the rapid increase in S. When S reached its final value (Epoch 2b), H also stabilized, albeit at a higher value ($H_{final} = 1.80$), maintaining approximately its initial baseline offset. Figure 2e,f shows a final example session in which S was decreased below 1. As was typical, H was greater than 1 in Epoch 1 ($H_{baseline} = 1.09$). When S was ramped down to 0.23 during Epoch 2a, H decreased accordingly for ~20 laps, appearing to plateau to a value slightly less than 1 for the remainder of Epoch 2a, and then further decreased to $H_{final} = 0.84$ in Epoch 2b. Thus, the change in H followed the direction of the change in S but did not decrease below ~0.84, even though S_{final} was much lower. Within any given session, individual place cells (distinct colors) fired at approximately the same location within the hippocampal frame of reference throughout that session (Fig. 2b,d,f, lower panels) due to strong internal coherence of the hippocampal map (Fig. 2g,h).

Across animals and sessions, the hippocampal gain at the end of Epoch 2 (after baseline subtraction, that is, $H_{final} - H_{baseline}$) was strongly related to the final stripe gain, S_{final}, in Epoch 2 (Fig. 2i). However, as illustrated by the examples in Fig. 2a–f, the relationship was not linear. For $S_{final} > 1$, the relationship was approximately linear with a slope of 0.57 (F test versus constant model: $P = 2.28 \times 10^{-5}$, $n = 18$, d.f. = 16), showing that there was reliable, but incomplete, modulation of the hippocampal gain by optic flow cues. However, for $S_{final} < 1$, the slope was 0.18 (F test versus constant model: $P = 0.036$, $n = 15$, d.f. = 13), much less than for $S_{final} > 1$. A power law empirically provided a good fit to the data (Fig. 2i); this nonlinear relationship indicates an important asymmetry in the affordance of optic flow over the hippocampal gain in upward versus downward directions and is consistent with an asymmetric influence

https://doi.org/10.1038/s41593-024-01681-9

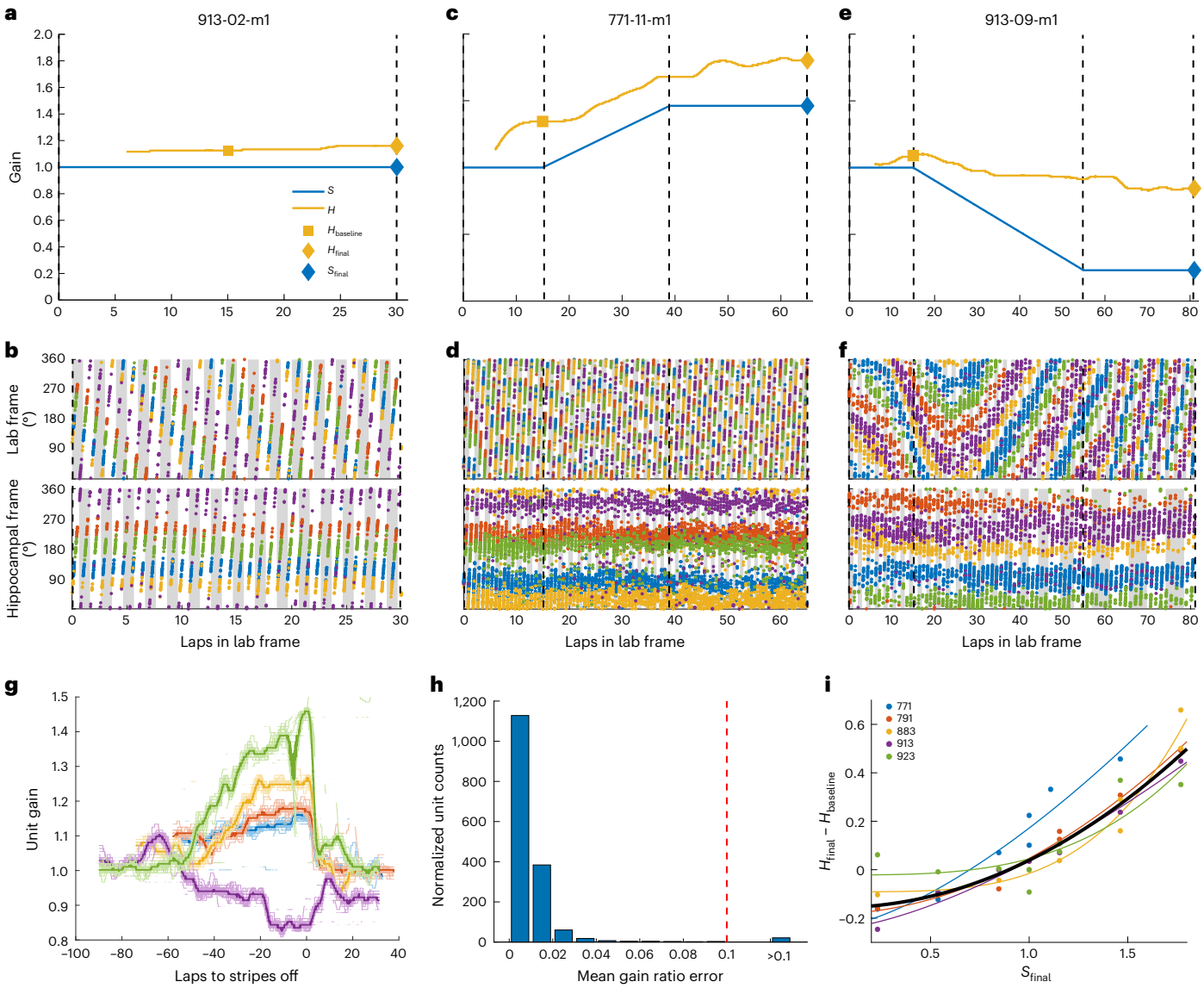

Fig. 2 | Effect of stripe manipulation on place cells. a, Session with $S = 1$ (stationary stripes; blue line). The hippocampal gain H (yellow line) drifted slightly, remaining above 1. Since H needs a six-window estimate, no value is plotted for the first six laps. **b**, Spikes from five units (distinct colors) plotted in the laboratory frame (top) and hippocampal frame (bottom) for the session in **a**. The hippocampal frame for each unit was computed by excluding that unit from the population. Units are coherent with each other, drift at the same rate and have aligned firing fields in the hippocampal frame. Alternating gray/white bars indicate laps in the respective frames. **c**, Session with $S_{final} > 1$. H initially increased and then settled towards the end of Epoch 1, but was driven upward when S increased. **d**, Same as **b**, but for the session in **c**. **e**, Session with $S_{final} < 1$. H was driven downward when S decreased, but not to the same extent as upward manipulation. **f**, Same as **b**, but for the session in **e**. **g**, Illustration of population gain coherence. Colors denote 5 d of open-loop sessions for rat 913 where $H_{final} \neq 1$. Light traces are gains H_i decoded from each unit, and dark traces are the medians of these values, defined as the population gain H. Sessions are aligned such that 0 is the end of Epoch 2b (stripes off). Gains from different units maintain a tight grouping in each session, demonstrating high coherence. **h**, Quantification of population gain coherence. If unit i was part of a coherent population, its gain H_i should equal the population gain H. The average gain ratio error $|1 - H_i/H|$ across all six-lap windows of a session is the coherence score for the unit (1,634 units, 65 sessions). To avoid bias, for each unit i, H_i was excluded from the computation of population gain H. Most units have scores close to zero and very few have values above 0.1 (0.10–0.42, 21 units). Most of the units fall in the first bin (error < 0.01, 1,128 units); they deviated no more than 2% from the median, likely within the range of measurement error. **i**, The change of H from its Epoch 1 baseline is a nonlinear function of the stripe manipulation, modeled by a power law (black line) $H_{final} - H_{baseline} = a + bS_{final}^{m}$ (fit parameters ± 95% confidence interval: $a = -0.16 \pm 0.07$, $b = 0.20 \pm 0.086$, $m = 2.05 \pm 0.66$; adjusted $r^2 = 0.86$, $n = 40$, d.f. = 37).

of optic flow reported in associated regions[42,51] (Extended Data Fig. 5 and 'Discussion'). This asymmetry can also cause a random drift biased towards higher gains in the presence of noisy velocity inputs (Extended Data Fig. 4c).

We also observe a consistent drift across $H_{baseline}$ sessions (Extended Data Fig. 4d). The baseline drift is linear and significant for all rats (positive for four rats and slightly negative for one rat; Extended Data Fig. 4e). The drift between sessions may be due to the accumulated biased within-session drift, but cannot be explained by the influence of the optic flow manipulation from the previous session (Extended Data Fig. 4f).

Recalibration of path integration without landmarks

Previously, we showed that imposing a sustained conflict between idiothetic path integration cues and movement relative to allothetic cues (that is, landmarks) induced recalibration of the path integration

https://doi.org/10.1038/s41593-024-01681-9

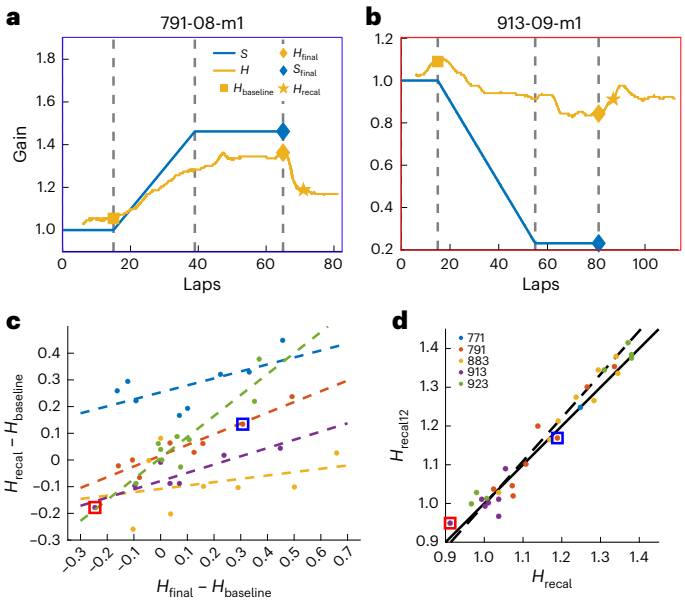

Fig. 3 | Recalibration of landmarks with open-loop optic flow. a, Gain curves for a session with S_{final} = 1.462 (*S* is blue line). The hippocampal gain *H* (yellow line) drifted upward during the manipulation to H_{final} = 1.36. In Epoch 3, the stripes were turned off (no blue line) and *H* dropped to 1.19, as measured by the value at the end of the first full six-lap window in the epoch (H_{recal}; star marker). **b**, Same as **a**, but for a session with S_{final} = 0.231. At the end of Epoch 2b, *H* dropped to H_{final} = 0.844 and, after stripes turned off, recovered to H_{recal} = 0.91. **c**, Baseline-subtracted H_{recal} versus H_{final}. Each data point is a session, colors denote sessions from individual rats and dashed lines are independent linear fits for each rat. The two sessions shown in **a** and **b** are enclosed in correspondingly colored boxes. Recalibration was significant across sessions and animals, as shown using an LME (see text). The individual animal fits had positive slopes for 5 of 5 rats and were significant for 3 of 5 rats (rat = 771, 791, 883, 913, 923; slope = 0.26, 0.40, 0.13, 0.31, 0.79; r^2 = 0.40, 0.86, 0.08, 0.76, 0.79; two-sided *t*-test against null hypothesis of slope zero, *t*-statistic = 2.00, 6.17, 0.71, 3.98, 5.19; $P = 0.093, 8.32 \times 10^{-4}, 0.507, 0.011, 1.27 \times 0^{-3}$; n = 8, 8, 8, 7, 9; d.f. = 6, 6, 6, 5, 7; no adjustment made for multiple comparisons). **d**, Maintenance of recalibrated value. In Epoch 3, the rats ran in the continued absence of stripe cues. We defined $H_{recal12}$ as the hippocampal gain value at lap 12, computed from the second six-lap window not overlapping with the first one in Epoch 3. Similar to **c**, data points denote sessions and colors denote rats. Linear fit to all data has slope 1.12 (dashed line; n = 39, d.f. = 37, two-sided *t*-test, *t*-statistic = 32.411, $P = 9.12 \times 10^{-29}$), very close to slope 1 (solid line), indicating that the recalibrated value was maintained in the absence of stripe cues in Epoch 3.

gain[6]. Thus, here we asked whether polarizing landmark information is necessary for this process, or if conflicting idiothetic cues alone could in fact induce such recalibration. Such an effect would demonstrate a previously unknown degree of plasticity in how various idiothetic pathways either mutually calibrate each other, or recalibrate a downstream circuit, to continuously fine-tune the path integrator without polarizing landmarks. At the end of Epoch 2b, during which optic flow was in continuous conflict with other idiothetic cues (for example, vestibular and motor efferent cues, whose perception is not altered by navigation in the Dome), we extinguished the stripes while leaving the overhead circular band of light to continue to illuminate the Dome (Epoch 3). If the manipulation of *H* during Epoch 2b was an immediate effect of cue manipulation, we would expect *H* to abruptly return to be near $H_{baseline}$. However, if instead the sustained manipulation induced a plastic alteration of the path integration process, as we previously found with landmarks[6], we would expect that, when the cues were removed, *H* would be partially recalibrated. The recalibrated gain H_{recal} was defined as the value of the hippocampal gain computed with the activity of the cells in the first six laps (the size of the moving spatial window used in gain estimation) after the stripes were extinguished.

Figure 3a shows an example of recalibration when *S* was increased to 1.46. The hippocampal gain *H* increased to H_{final} = 1.36 by the end of Epoch 2b. When the stripes were extinguished in Epoch 3, the hippocampal gain decreased to H_{recal} = 1.19, above its baseline in Epoch 1 ($H_{baseline}$ = 1.06). Figure 3b shows an example in which *S* was decreased to 0.231. *H* showed a typical increase over laps in Epoch 1, which began to reverse when *S* began to decrease in Epoch 2, reaching an initial plateau around 0.95 in Epoch 2a and then jumping to a new plateau around H_{final} = 0.84 in Epoch 2b. When the stripes were extinguished in Epoch 3, *H* maintained a value around H_{recal} = 0.91, below its baseline in Epoch 1 ($H_{baseline}$ = 1.09).

We observed modest but reliable recalibration across sessions (Fig. 3c). A linear mixed-effects model (LME) with ($H_{recal} - H_{baseline}$) as the dependent variable, ($H_{final} - H_{baseline}$) as a fixed-effect independent variable and rat identity as a random-effect independent variable showed a significant slope of 0.32 (two-sided *t*-test; n = 40, d.f. = 39, *t*-statistic = 5.25, $P = 5.7 \times 10^{-6}$). Note that the statistical tests were performed after subtracting the baseline offset from each session, to assess the relationship between changes in hippocampal gains. We also fit a model with S_{final} as the fixed-effect independent variable; the slope between ($H_{recal} - H_{baseline}$) and S_{final} was 0.11 (two-sided *t*-test; n = 40, d.f. = 39, *t*-statistic = 3.97, $P = 3 \times 10^{-4}$). The difference in the Bayesian information criterion (BIC)[52] between the two models ($H_{final} - H_{baseline}$: BIC = −61.28; S_{final}: BIC = −53.49) suggests that the internal hippocampal dynamics H_{final} was a better predictor of the hippocampal gain H_{recal} than was the external sensory input S_{final}. Since stripe gain increased or decreased monotonically during each session with $S_{final} \neq 1$, we also tested how time and distance run affected the evolution of $H - H_{baseline}$ (Extended Data Fig. 6b). We considered the minimum distance (49 laps) and the minimum time (13.1 min) that stripe manipulation lasted across all open-loop sessions with $S_{final} \neq 1$. At 49 laps, there was no significant relationship between $H - H_{baseline}$ and time. At 13.1 min, there was no significant relationship between $H - H_{baseline}$ and distance. In both cases, there was a power-law relationship between $H - H_{baseline}$ and stripe gain *S* (Extended Data Fig. 6c,d).

We examined whether the recalibration effect was maintained over many laps by tracking the hippocampal gain across Epoch 3 (Fig. 3d). There was a near one-to-one correspondence between the hippocampal gain at laps 6 and 12 in Epoch 3. This correspondence shows that the optic flow-based hippocampal gain manipulation induced a long-term recalibration of path integration with respect to the other idiothetic cues (for example, vestibular cues, proprioceptive cues or motor copy) that presumably drove the path integration process when the stripes were extinguished in Epoch 3.

Closed-loop cognitive clamp stabilizes path integration

Despite the clear, bidirectional influence of optic flow on place cells, the precision of its control over the place fields was variable (Extended Data Fig. 5b) and offset by significant shifts of the baseline gain within and across sessions (Extended Data Fig. 4). This imprecision contrasts with the powerful control typically exerted by salient landmarks in the environment[3,6,9,10]. We investigated whether we could mimic the strong control by landmarks with pure optic flow information by using concepts from control theory to clamp the hippocampal gain to a desired value. Specifically, we created a neural feedback control loop in which CA1 place cell activity was used to adjust the experimental stripe gain, *S*, in real time to drive the hippocampal gain to an experimentally chosen desired value, $H_{desired}$ (Fig. 4a).

This control scheme compares a real-time, neurally decoded estimate of the hippocampal gain, $\hat{H}$, with the desired hippocampal gain, $H_{desired}$, and feeds their difference back through an integral control law that automatically adjusts the stripe gain:

$$S = K_I \int_{\theta_0}^{\theta} (H_{desired} - \hat{H})\, d\vartheta$$

Here, θ denotes the cumulative, unwrapped angular displacement of the rat (measured in units of laps) and ϑ is a dummy variable of integration. The value of S was initialized to 1 at the beginning of Epoch 2. The controller constant, K_I, known as the integral gain in control theory, was designed to stabilize the closed-loop system based on a simplified model that considers the six-lap windowing of our real-time hippocampal gain estimate (Methods and Extended Data Fig. 7). Intuitively, an integral control law continuously increases or decreases the strength of the control signal (that is, S) until the feedback error is extinguished. The integral control law created smooth changes in the stripe gain; that is, a gradual 'ramp' emerged that is qualitatively similar to the preprogrammed stripe gain ramp presented in Epoch 2a of our open-loop experiments (Fig. 2). This gradual ramp avoided sudden changes in optic flow velocity as might result from other control schemes (for example, proportional or derivative controllers).

The integral controller modulated S at 1-s intervals with $K_I = 0.2$ (Methods). The control law was implemented on four animals across a total of 25 closed-loop sessions (mean 36 units per session, range 2–74 units). Figure 4b depicts an example session in which H was initially greater than 1 ($H_{baseline} = 1.248$) and $H_{desired}$ was set to 1. The controller gradually reduced the stripe gain based on the integral control law, evidently causing a percept to the animal that it was moving progressively slower, until ultimately the hippocampal gain returned to unity ($H_{final} = 1.037$). In steady state, a population of simultaneously recorded place cells largely stabilized itself relative to the track (Fig. 4c), even in the absence of salient landmarks.

Our controller was successful in stabilizing the hippocampal gain to the desired value for a large fraction of sessions in which $H_{desired} > 1$ (Extended Data Fig. 8). Figure 4d depicts an example in which the hippocampal gain was gradually ramped up to a desired value of 1.769 via the integral controller and stabilized around that value for approximately 45 laps ($H_{final} = 1.784$). As can be seen in Fig. 4e, a population of simultaneously recorded neurons became relatively stable in an artificial reference frame that rotated according to the desired gain, demonstrating the effectiveness of the control law. The control law was generally not successful in completely stabilizing to $H_{desired} < 1$, although there was often still an influence of the control law (Fig. 4f,g). This result parallels the relatively modest effect for $S < 1$ described earlier in open-loop experiments (Fig. 2e,f,i and Extended Data Fig. 5a). To assess the overall control law's effectiveness, we assessed H_{final} at the end of Epoch 2 with $H_{desired}$, after subtracting baseline from both variables (Fig. 4h). Most data points were close to the unity diagonal between these values, demonstrating that our neurally closed-loop controller was able to systematically command the rate of updating of the hippocampal map using purely optic flow cues. Further analysis of the closed-loop controller's effectiveness is shown in Extended Data Figs. 5c and 6a.

We next tested whether recalibration of path integration by optic flow was also observed in closed-loop control sessions by examining the path integration gain after the stripes were extinguished (Epoch 3). We restricted our analysis to cases where the control law was successful in driving H to the desired value (Methods and Extended Data Fig. 8; ten strongly controlled and nine modestly controlled sessions). We further excluded rat 923 from analysis, as the three cases of strongly and modestly controlled sessions from this rat came from sessions in which the values of ($H_{desired} - H_{baseline}$) were clustered too close to provide a meaningful measurement of trend; this exclusion produced no meaningful differences in the results. Two example sessions (Fig. 5a, strong control, and Fig. 5b, modest control) illustrate the effect of the recalibration, as there is a residual effect in Epoch 3 of the gain control manipulation carried out in Epoch 2. Similar to open-loop trials, a linear mixed-effects model analysis across the three animals, with ($H_{recal} - H_{baseline}$) as the dependent variable, ($H_{final} - H_{baseline}$) as a fixed-effect independent variable and rat identity as a random-effect independent variable, demonstrated that there was a modest but reliable relationship between these variables (slope = 0.38; two-sided t-test; $n = 16$, d.f. = 15, t-statistic = 8.94, $P = 2.15 \times 10^{-7}$). The slope between ($H_{recal} - H_{baseline}$) and S_{final} was 0.12 (two-sided t-test; $n = 16$, d.f. = 15, t-statistic = 3.31, $P = 4.8 \times 10^{-3}$). Again, the internal dynamics H_{final} was a stronger predictor of H_{recal} than was the sensory input S_{final} ($H_{final} - H_{baseline}$: BIC = −38.4; S_{final}: BIC = −19.6)[52]. The value of H_{recal} was stable across many laps in Epoch 3 (Fig. 5d). Interestingly, the hippocampal gain in rat 883 showed a strong rebound when the stripes were extinguished, leading to a marked offset in the linear fit to the recalibration (Fig. 5c, yellow dots) that was similar to what occurred for that animal in open-loop (Fig. 3c, yellow dots). Nonetheless, this animal still showed a significant, positive slope between H_{recal} and H_{final}.

Discussion

Optic flow is an idiothetic cue that is often hypothesized to be a major influence on place cells but which has not been studied extensively and parametrically in this regard. We used a virtual reality apparatus with a freely moving rat to demonstrate systematic control of place cells by optic flow, analogous to the well-documented control exerted by allothetic cues such as landmarks[3,6,7,10–13]. Under natural conditions, salient landmarks and boundaries anchor the internal reference frame of the hippocampus, making it difficult to study the influence of idiothetic cues in isolation and almost impossible to quantify how conflicting idiothetic cues interact in updating the path integration computation[1,2,15,53]. Our previous work showed that allothetic information can provide a teaching signal to recalibrate the path integration system[6]. In that case, the teaching signal—the landmarks—provided an absolute positional signal in its frame of reference that anchored the internal, hippocampal frame of reference. Idiothetic cues, in contrast, can provide only relative positional signals (that is, updating a positional signal relative to the previous estimate of position). Does the path integration system require an absolute position teaching signal to calibrate its gain, or could relative signals from different idiothetic sources calibrate each other? The experiments reported here establish that manipulation of optic flow can induce recalibration of the path integrator in a similar way to what we had previously shown by landmark manipulations.

Optic flow cues exerted substantially less influence over the hippocampal representation of position than landmarks in the same apparatus[6]. With landmarks, the place cell population typically remained anchored to the landmark-centered reference frame[6]. With stripes, by contrast, the hippocampal representation of position drifted relative to a stripe frame of reference, often quite substantially, in the absence of stabilizing landmarks. The weaker influence of optic flow compared to landmarks was nevertheless sufficient for a new, model-based, neurally closed-loop controller to succeed in driving the hippocampal gain to a desired value in a majority of sessions, sometimes maintaining a desired value for dozens of laps (Extended Data Fig. 5c). These results revealed a striking degree of influence of optic flow on place cells.

The influence of optic flow cues on the hippocampal map was asymmetric (Fig. 2i and Extended Data Fig. 5a), in that it was easier to increase the hippocampal gain than reduce it. This finding is akin to our previous results[6] with landmarks, in which the place map was unlikely to break away from the landmark cues when the visual gain was increased but was much more likely to break away from landmark cues when the visual cue gain was reduced. Other groups have reported similar asymmetries in 'up' versus 'down' influence of perceptual manipulations over entorhinal populations[51] and behavior[40], but what these biases reveal about the nature of computations underlying path integration remains an open question and may play a role in the tendency for path integration to overestimate the distance traveled[49,50].

The data and modeling efforts by Campbell and colleagues[51] indicate that this asymmetry might arise from a gain-dependent weighting of visual and locomotor speed cues in the velocity input. It is possible that the salience of the reduced-gain cue is less than the increased-gain cue because it creates a lower relative optic flow velocity, and that such a

https://doi.org/10.1038/s41593-024-01681-9

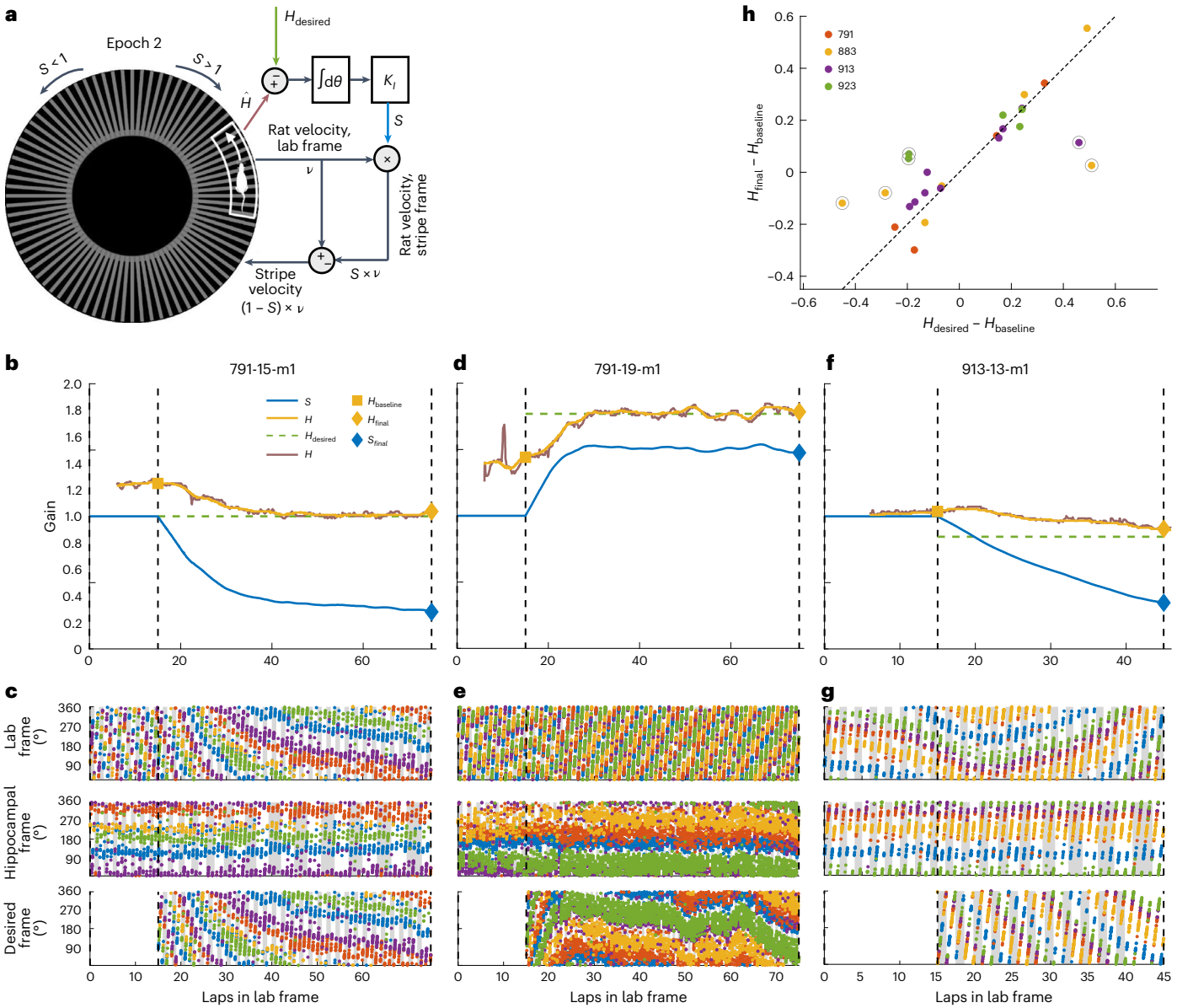

Fig. 4 | Cognitive clamp of hippocampal gain via optic flow. a, Schematic of closed-loop controller. Similar to Fig. 1c, except that during Epoch 2, the stripe gain S was continually updated using a neurally closed-loop integral controller, which was designed to clamp the estimated hippocampal gain $\hat{H}$ to the desired value $H_{desired}$. **b**, Example of closed-loop control to $H_{desired} = 1$. The stripe gain S (blue), real-time hippocampal gain estimate $\hat{H}$ (brown), offline hippocampal gain H decoded postexperiment (yellow) and desired hippocampal gain $H_{desired}$ (dashed green line) are plotted against laps the rat ran in the laboratory frame. $H_{baseline}$ was the hippocampal gain in Epoch 1 (before onset of the controller) and H_{final} was the hippocampal gain at the end of Epoch 2. In this session, $H_{baseline}$ was ~1.25. When the controller was activated, the stripe gain became lower, driving the hippocampal gain to $H_{desired} = 1$ by ~lap 40 and maintaining it there throughout the remainder of Epoch 2. **c**, Spikes from five units for the session in **b**. Top, middle and bottom graphs show the place fields in the lab, hippocampal and desired reference frames, respectively. The hippocampal frame was computed using a population gain that excluded the gain of the unit being plotted. The desired reference frame was computed by integration: $\int H_{desired}\, d\theta = H_{desired}\, \theta$ (since $H_{desired}$ was constant). There are no points in the desired frame in Epoch 1 as the controller was not activated until Epoch 2. Since $H_{desired} = 1$, the lab and desired frame plots are identical during Epoch 2. **d**, Closed-loop control to $H_{desired} = 1.77$. **e**, Raster plots for five place fields from the experiment in **d**. **f**, Closed-loop control to $H_{desired} = 0.85$. In this example, H in Epoch 1 was only slightly higher than 1 and rising. In Epoch 2, the controller reversed the rise in H and gradually moved it closer to $H_{desired}$. Although the controller was unable to bring H to $H_{desired}$, H was nonetheless driven below 1 and still decreasing at the end of Epoch 2. **g**, Raster plots for five place fields from the experiment in **f**. **h**, H_{final} versus $H_{desired}$ for all four rats who underwent closed-loop sessions, with $H_{baseline}$ subtracted. Most sessions lie close to unity (dashed diagonal), indicating control of the hippocampal gain. Points away from the diagonal denote uncontrolled sessions (circled) (Methods).

decrease in salience leads to a decrease in its sensory weight within a cue integration framework[51,54]. Indeed, as the stripe gain approaches 0 (we never let it get to zero itself), the absolute optic flow the animal experiences decreases, as the stripes are moving closer and closer to the animal's velocity. This might result in a further threshold nonlinearity where the inputs are not considered optic flow at all. Additionally, there is an asymmetry in the experimental manipulation. For example, decreasing the optic flow gain from 1 to 0 eliminates stripe-based optic flow and would require an infinite number of steps to progress the same distance in visual space. By contrast, increasing the gain the same amount, from 1 to 2, merely doubles the optic flow speed, requiring half the number of steps. This hyperbolic relationship between change in stripe gain and the required number of steps to progress in the virtual frame of reference may partially explain the asymmetric influence of optic flow gain.

https://doi.org/10.1038/s41593-024-01681-9

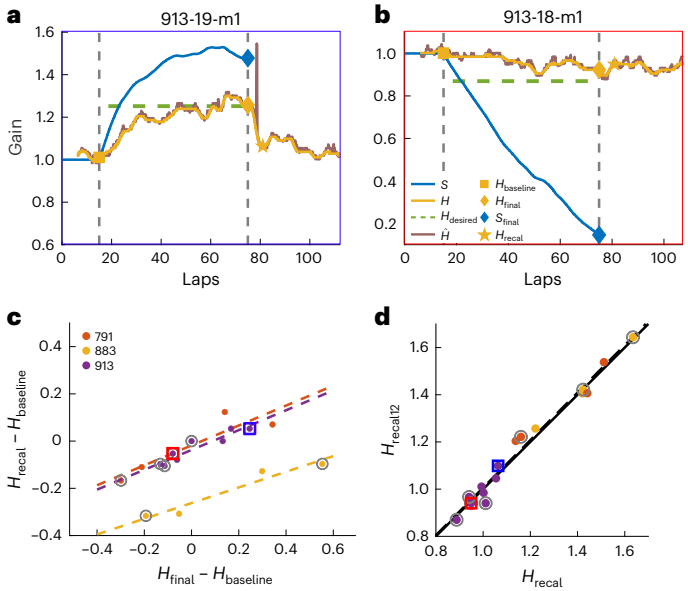

Fig. 5 | Recalibration of path integration gain via the cognitive clamp. **a**, Recalibration to $H > 1$. The closed-loop controller drove the hippocampal gain H to $H_{desired} = 1.25$. When the stripes were turned off at lap 75, H was reduced to ~1.06, which was higher than the baseline gain in Epoch 1 ($H_{baseline} = 1.00$). **b**, Recalibration to $H < 1$. This example comes from the same animal as in **a** on the previous day, in which $H_{desired}$ was set at 0.87. The hippocampal gain was maintained at $H = 1$ for 15 laps in the absence of landmarks, and the gain was reduced to slightly below 1 for ~20 laps when the controller was activated. At lap 45, the hippocampal gain started to decrease further and reached $H_{desired} = 0.92$. When the stripes were turned off at lap 75, the hippocampal gain was maintained near this value ($H_{recal} = 0.95$). **c**, Hippocampal gain after recalibration ($H_{recal} - H_{baseline}$) as a function of the final hippocampal gain ($H_{final} - H_{baseline}$) for the sessions from three rats (data points denote sessions, colors denote rats) in which the stripes strongly controlled the hippocampal gain in Epoch 2. For all three rats, there was a significant, linear relationship between H_{recal} and H_{final} (with $H_{baseline}$ subtracted from both variables), as measured using an LME (see text). Modestly controlled sessions are circled in gray. Linear fits (dashed lines) were positive and significant for 2 of 3 animals (rat = 791, 883, 913; slope = 0.42, 0.33, 0.42; $r^2 = 0.80, 0.92, 0.86$; two-sided t-test against null hypothesis of slope 0, t-statistic = 2.86, 4.86, 6.06; $P = 0.104, 0.040, 0.001$; $n = 4, 4, 8$; d.f. = 2,2,6; no adjustment made for multiple comparisons). **d**, Maintenance of H_{recal} over laps. Data points denote sessions and colors denote rats, similar to **c**. Across sessions, there was a strong relationship close to unity between the values of H_{recal} measured 6 laps and 12 laps after the stripes were turned off (slope = 1.007, $r^2 = 0.98$; two-sided t-test, t-statistic = 32.371, $P = 1.02 \times 10^{-16}$, $n = 19$, d.f. = 17).

Further insight into the asymmetry might be gained from studying the activity in brain regions such as the anterolateral cortical field (AL) and the lateral posterior thalamic nucleus (LP) of rodents. The AL is a higher-order visual processing region with strong inputs to the dorsal stream[55] via the posterior parietal cortex and the medial entorhinal cortex, while the LP (the homolog of the pulvinar in primates and a strong input to the AL) has been implicated in visuomotor integration. The LP contains visuomotor error signals between locomotion cues and optic flow[56]. Interestingly, the AL neurons and LP boutons in AL showed predominantly positive correlations with optic flow speed and negative correlations with running speed[57], implying that they are activated by visual flow and suppressed by locomotion. Blot and colleagues[57] inferred that an example case under which these neurons would be most active is when optic flow speed is higher than expected based on the animal's running speed, a condition instantiated by an increasing stripe gain in this study. Such an elevated activity might play a role in the asymmetric influence of optic flow on the hippocampal map.

Mixed-effects models established that the best predictor of the recalibrated gain was not the final stripe gain, S_{final}, but rather the final hippocampal gain itself, H_{final}. This finding provides evidence that, while the optic flow cues may substantially influence the hippocampal gain, they may only indirectly lead to recalibration. In other words, sensory perturbations (S_{final}) vary in the extent to which they alter the hippocampal gain (H), but as this altered gain is maintained over time, it is the hippocampal dynamics (H_{final}), not the sensory input, that might ultimately drive the persistent change in the underlying computation that manifests as a new, recalibrated gain after the stimulus is removed (H_{recal}). Since stripe gain is more salient in the up sessions, it is possible that recalibration in these sessions is more directly driven by the sensory input. However, this effect is also difficult to isolate due to the linear correlation between S_{final} and the change in hippocampal gain ($H_{final} - H_{baseline}$) in the up sessions.

Robust internal dynamics are a hallmark of hippocampal circuitry. Our research shows that the internal dynamics of the path integration network are constantly being fine-tuned in relation to potentially conflicting streams of idiothetic information. Specifically, the optic flow cues that we manipulated were placed in conflict with other idiothetic cues (for example, vestibular cues, proprioceptive cues, motor efference copy) that serve as inputs to the path integration system but were not directly affected by the optic flow changes. Our recordings from CA1 place cells are a reflection of the results of the path integration computation, which might occur upstream of the hippocampus[14]. Importantly, a global, top-down teaching signal that binds the hippocampal frame of reference to an absolute external frame of reference is not required for recalibration. Instead, the internal dynamics are the reference frame against which idiothetic inputs are compared, providing an externally ungrounded teaching signal. Loosely speaking, multimodal cue integration[54,58] and recalibration of path integration are reminiscent of clock synchronization and recalibration[59]. In the presence of a trusted master timekeeper (for example, an atomic clock), drifting clocks are 'latched' onto it, and their rates of drift are corrected—much like visual landmarks anchor the spatial representation and induce path integrator recalibration[6]. In the absence of this master clock, synchronization algorithms rely on a network of clocks synchronizing and calibrating each other—much like optic flow influences (without anchoring) the spatial representation, nevertheless inducing recalibration.

By stabilizing the hippocampal representation in the absence of allothetic landmarks, the neurally closed-loop controller we developed opens the door for studying idiothetic inputs to the hippocampus with a degree of control previously reserved for studies of allothetic inputs. The present study used an online decoder and controller to calculate and manipulate the hippocampal gain, but future work will likely be able to decode the hippocampal representation of the actual position of the animal in real time[60,61] and control directly the internal sense of location expressed by hippocampal and parahippocampal activity based purely on idiothetic cues. Furthermore, the relative influence of different idiothetic cues can be determined in ways analogous to classic voltage clamp studies. That is, one idiothetic input (for example, vestibular) can be manipulated systematically, and the other (for example, optic flow) can be adjusted to counter the manipulation and clamp the hippocampal representation. The magnitude of the controller input required to clamp the representation is a measure of the relative strength of the two cues' influence on the updating of position on the hippocampal map, much like the current required to maintain the voltage clamp at a set value indicates the relative current flow through various ion channels[23]. Such neurally closed-loop experiments that regulate or stabilize internal variables can generalize to other fields of cognitive neuroscience in which high-order neural representations (for example, evidence accumulation, motor intentions or attention) are influenced by, but not necessarily bound to, external sensory input and are instead dynamically modulated by internal variables.

Online content

Any methods, additional references, Nature Portfolio reporting summaries, source data, extended data, supplementary information, acknowledgements, peer review information; details of author contributions and competing interests; and statements of data and code availability are available at https://doi.org/10.1038/s41593-024-01681-9.

References

1. Etienne, A. S. & Jeffery, K. J. Path integration in mammals. *Hippocampus* **14**, 180–192 (2004).
2. McNaughton, B. L. et al. Deciphering the hippocampal polyglot: the hippocampus as a path integration system. *J. Exp. Biol.* **199**, 173–185 (1996).
3. O'Keefe, J. & Conway, D. H. Hippocampal place units in the freely moving rat: why they fire where they fire. *Exp. Brain Res.* **31**, 573–590 (1978).
4. Knierim, J. J., Kudrimoti, H. S. & McNaughton, B. L. Place cells, head direction cells, and the learning of landmark stability. *J. Neurosci.* **15**, 1648–1659 (1995).
5. Knierim, J. J., Kudrimoti, H. S. & McNaughton, B. L. Interactions between idiothetic cues and external landmarks in the control of place cells and head direction cells. *J. Neurophysiol.* **80**, 425–446 (1998).
6. Jayakumar, R. P. et al. Recalibration of path integration in hippocampal place cells. *Nature* **566**, 533–537 (2019).
7. Chen, G., King, J. A., Burgess, N. & O'Keefe, J. How vision and movement combine in the hippocampal place code. *Proc. Natl Acad. Sci. USA* **110**, 378–383 (2013).
8. Terrazas, A. et al. Self-motion and the hippocampal spatial metric. *J. Neurosci.* **25**, 8085–8096 (2005).
9. Moser, E. I., Moser, M.-B. & McNaughton, B. L. Spatial representation in the hippocampal formation: a history. *Nat. Neurosci.* **20**, 1448–1464 (2017).
10. Muller, R. U. & Kubie, J. L. The effects of changes in the environment on the spatial firing of hippocampal complex-spike cells. *J. Neurosci.* **7**, 1951–1968 (1987).
11. Knierim, J. J. & Hamilton, D. A. Framing spatial cognition: neural representations of proximal and distal frames of reference and their roles in navigation. *Physiol. Rev.* **91**, 1245–1279 (2011).
12. Acharya, L., Aghajan, Z. M., Vuong, C., Moore, J. J. & Mehta, M. R. Causal influence of visual cues on hippocampal directional selectivity. *Cell* **164**, 197–207 (2016).
13. Purandare, C. S. et al. Moving bar of light evokes vectorial spatial selectivity in the immobile rat hippocampus. *Nature* **602**, 461–467 (2022).
14. McNaughton, B. L., Battaglia, F. P., Jensen, O., Moser, E. I. & Moser, M. B. Path integration and the neural basis of the 'cognitive map'. *Nat. Rev. Neurosci.* **7**, 663–678 (2006).
15. Savelli, F. & Knierim, J. J. Origin and role of path integration in the cognitive representations of the hippocampus: computational insights into open questions. *J. Exp. Biol.* **222**, jeb188912 (2019).
16. Zhang, S., Schönfeld, F., Wiskott, L. & Manahan-Vaughan, D. Spatial representations of place cells in darkness are supported by path integration and border information. *Front. Behav. Neurosci.* **8**, 222 (2014).
17. Madhav, M. S. & Cowan, N. J. The synergy between neuroscience and control theory: the nervous system as inspiration for hard control challenges. *Annu. Rev. Control Robot. Auton. Syst.* **3**, 243–267 (2020).
18. Cowan, N. J. et al. Feedback control as a framework for understanding tradeoffs in biology. *Integr. Comp. Biol.* **54**, 223–237 (2014).
19. Marken, R. S. & Mansell, W. Perceptual control as a unifying concept in psychology. *Rev. Gen. Psychol.* **17**, 190–195 (2013).
20. Robinson, D. A. The use of control systems analysis in the neurophysiology of eye movements. *Annu. Rev. Neurosci.* **4**, 463–503 (1981).
21. McNamee, D. & Wolpert, D. M. Internal models in biological control. *Annu. Rev. Control Robot. Auton. Syst.* **2**, 339–364 (2019).
22. Wiener, N. *Cybernetics or Control and Communication in the Animal and the Machine* (MIT, 2019).
23. Huxley, A. From overshoot to voltage clamp. *Trends Neurosci.* **25**, 553–558 (2002).
24. Peixoto, D. et al. Decoding and perturbing decision states in real time. *Nature* **591**, 604–609 (2021).
25. Wright, J., Macefield, V. G., Schaik, Avan. & Tapson, J. C. A review of control strategies in closed-loop neuroprosthetic systems. *Front. Neurosci.* **10**, 312 (2016).
26. O'Doherty, J. E. et al. Active tactile exploration using a brain-machine-brain interface. *Nature* **479**, 228–231 (2011).
27. Ruffini, G. Conscious brain-to-brain communication using noninvasive technologies. in *Closed Loop Neuroscience* (El Hady, A. ed) 241–256 (Academic Press, 2016).
28. Roth, E., Sponberg, S. & Cowan, N. J. A comparative approach to closed-loop computation. *Curr. Opin. Neurobiol.* **25**, 54–62 (2014).
29. Mohler, B. J. et al. Calibration of locomotion resulting from visual motion in a treadmill-based virtual environment. *ACM Trans. Appl. Percept.* **4**, 4-es (2007).
30. Tcheang, L., Bülthoff, H. H. & Burgess, N. Visual influence on path integration in darkness indicates a multimodal representation of large-scale space. *Proc. Natl Acad. Sci. USA* **108**, 1152–1157 (2011).
31. Rieser, J. J., Pick, H. L., Ashmead, D. H. & Garing, A. E. Calibration of human locomotion and models of perceptual-motor organization. *J. Exp. Psychol. Hum. Percept. Perform.* **21**, 480–497 (1995).
32. Madhav, M. S. et al. The Dome: a virtual reality apparatus for freely locomoting rodents. *J. Neurosci. Methods* **368**, 109336 (2022).
33. Kautzky, M. & Thurley, K. Estimation of self-motion duration and distance in rodents. *R. Soc. Open Sci.* **3**, 160118 (2016).
34. O'Connor, S. M. & Donelan, J. M. Fast visual prediction and slow optimization of preferred walking speed. *J. Neurophysiol.* **107**, 2549–2559 (2012).
35. Warren, W. H., Kay, B. A., Zosh, W. D., Duchon, A. P. & Sahuc, S. Optic flow is used to control human walking. *Nat. Neurosci.* **4**, 213–216 (2001).
36. Bruggeman, H., Zosh, W. & Warren, W. H. Optic flow drives human visuo-locomotor adaptation. *Curr. Biol.* **17**, 2035–2040 (2007).
37. Srinivasan, M. V., Zhang, S. W., Lehrer, M. & Collett, T. S. Honeybee navigation en route to the goal: visual flight control and odometry. *J. Exp. Biol.* **199**, 237–244 (1996).
38. Pfeffer, S. E. & Wittlinger, M. Optic flow odometry operates independently of stride integration in carried ants. *Science* **353**, 1155–1157 (2016).
39. Webb, B. & Wystrach, A. Neural mechanisms of insect navigation. *Curr. Opin. Insect Sci.* **15**, 27–39 (2016).
40. Biswas, D. et al. Closed-loop control of active sensing movements regulates sensory slip. *Curr. Biol.* **28**, 4029–4036.e4 (2018).
41. Smyth, G., Baliga, V. B., Gaede, A. H., Wylie, D. R. & Altshuler, D. L. Specializations in optic flow encoding in the pretectum of hummingbirds and zebra finches. *Curr. Biol.* https://doi.org/10.1016/j.cub.2022.04.076 (2022).
42. Mao, D., Molina, L. A., Bonin, V. & McNaughton, B. L. Vision and locomotion combine to drive path integration sequences in mouse retrosplenial cortex. *Curr. Biol.* **30**, 1680–1688.e4 (2020).
43. Arleo, A. et al. Optic flow stimuli update anterodorsal thalamus head direction neuronal activity in rats. *J. Neurosci.* **33**, 16790–16795 (2013).
44. Sharp, P. E., Blair, H. T., Etkin, D. & Tzanetos, D. B. Influences of vestibular and visual motion information on the spatial firing patterns of hippocampal place cells. *J. Neurosci.* **15**, 173–189 (1995).

45. Gaede, A. H. et al. Response properties of optic flow neurons in the accessory optic system of hummingbirds versus zebra finches and pigeons. *J. Neurophysiol.* **127**, 130–144 (2022).
46. Mertes, M., Dittmar, L., Egelhaaf, M. & Boeddeker, N. Visual motion-sensitive neurons in the bumblebee brain convey information about landmarks during a navigational task. *Front. Behav. Neurosci.* **8**, 335 (2014).
47. Yu, C. P., Page, W. K., Gaborski, R. & Duffy, C. J. Receptive field dynamics underlying MST neuronal optic flow selectivity. *J. Neurophysiol.* **103**, 2794–2807 (2010).
48. Greenlee, M. W. Human cortical areas underlying the perception of optic flow: brain imaging studies. *Int. Rev. Neurobiol.* **44**, 269–292 (2000).
49. Stangl, M., Kanitscheider, I., Riemer, M., Fiete, I. & Wolbers, T. Sources of path integration error in young and aging humans. *Nat. Commun.* **11**, 2626 (2020).
50. Seguinot, V., Cattet, J. & Benhamou, S. Path integration in dogs. *Anim. Behav.* **55**, 787–797 (1998).
51. Campbell, M. G. et al. Principles governing the integration of landmark and self-motion cues in entorhinal cortical codes for navigation. *Nat. Neurosci.* **21**, 1096–1106 (2018).
52. Raftery, A. E. Bayesian model selection in social research. *Sociol. Methodol.* **25**, 111 (1995).
53. Samsonovich, A. & McNaughton, B. L. Path integration and cognitive mapping in a continuous attractor neural network model. *J. Neurosci.* **17**, 5900–5920 (1997).
54. Carver, S., Kiemel, T. & Jeka, J. J. Modeling the dynamics of sensory reweighting. *Biol. Cybern.* **95**, 123–134 (2006).
55. Wang, Q., Gao, E. & Burkhalter, A. Gateways of ventral and dorsal streams in mouse visual cortex. *J. Neurosci.* **31**, 1905–1918 (2011).
56. Roth, M. M. et al. Thalamic nuclei convey diverse contextual information to layer 1 of visual cortex. *Nat. Neurosci.* **19**, 299–307 (2016).
57. Blot, A. et al. Visual intracortical and transthalamic pathways carry distinct information to cortical areas. *Neuron* **109**, 1996–2008.e6 (2021).
58. Fetsch, C. R., DeAngelis, G. C. & Angelaki, D. E. Bridging the gap between theories of sensory cue integration and the physiology of multisensory neurons. *Nat. Rev. Neurosci.* **14**, 429–442 (2013).
59. Contzen, M. P. Consensus based synchronization of clocks to diminish the effect of clock drifts in microgrids. *IFAC Pap OnLine* **53**, 12980–12985 (2020).
60. Kloosterman, F., Layton, S. P., Chen, Z. & Wilson, M. S. Bayesian decoding using unsorted spikes in the rat hippocampus. *J. Neurophysiol.* **111**, 217–227 (2014).
61. Hu, S. et al. Real-time readout of large-scale unsorted neural ensemble place codes. *Cell Rep.* **25**, 2635–2642.e5 (2018).

https://doi.org/10.1038/s41593-024-01681-9

Methods

Subjects

Five Long–Evans rats (Envigo Harlan; three males (numbers 771, 791 and 883) and two females (numbers 913 and 923)) were housed individually on a 12/12-h light/dark cycle. There were no obvious differences in results between male and female rats, and the data are reported by rat as appropriate in the results. All training and experiments were conducted during the dark portion of the cycle. The rats were 5–8 months old and weighed 300–450 g at the time of surgery. All animal care and housing procedures complied with National Institutes of Health guidelines and followed protocols approved by the Institutional Animal Care and Use Committee at Johns Hopkins University.

Dome apparatus

To present visual landmarks and optic flow cues to the rat, we used our custom planetarium-like virtual reality apparatus, the Dome (see ref. 32 for details on the design and construction). Briefly, rats locomoted near the outer periphery of an annular table (152.4-cm outer diameter, 45.7-cm inner diameter) centered within the dome. The image from a projector (G7500UNL, Epson) fitted with a long-throw lens (ELPLM11, Epson) was reflected off a plane mirror (152 × 152 × 12.7 mm^3, First Surface Mirror) and a hemispherical mirror (254-mm diameter, 150-mm radius of curvature, 40/20 surface quality, 1/4-wave accuracy, protected aluminum coating, Cumberland Optical) mounted at the center of the Dome. The resulting image covered the inside surface of the Dome shell, providing a projected view to the rat 360° in azimuth and almost 90° in elevation. A near-infrared camera (GS3-U3–41C6NIR-C, FLIR; 2,048 × 2,048 pixels, 45 frames per second) with a wide-field lens (NMV-6M1, 6 mm, F1.8, Navitar) provided an overhead view of the experiment. The three-dimensional position and orientation of the head of the rat were detected in real time (45 frames per s) through single-camera tracking[62] of a set of markers mounted on the rat's neural recording implant. The central rotating pillar of the dome was mounted on bearings. An enclosure, attached to the central pillar via radial boom arms, covered a 45° region around the rat. The central pillar along with the enclosure were moved using a motor in response to the rat's position, such that the rat was kept near the center of the enclosure. The enclosure was moved only when the rat moved forward (CCW) and not when it went backwards (CW)—this encouraged continuous forward running. A micro-peristaltic pump (RP-Q1, Taskago Fluidics) on the central pillar dropped liquid reward (50% diluted Ensure®) through a feed tube routed to the front of the enclosure. A plastic spreader and paper towels were attached to a third radial boom arm mounted to the central pillar opposite from the enclosure. This cleaning arm wiped up or spread out the scent of urine and uneaten food, as well as pushed feces off the table, reducing the salience and stability of local olfactory cues. All the nonprojected visual cues available to the rat were either circularly symmetric (nonpolarizing) or moved along with the rat.

Projected visual cues

During Epochs 1 and 2, a set of 80 equally spaced white stripes was projected into the dome to form the optic flow cue. The stripes were each 1.5° wide and 40° high, centered at 45° elevation. The spacing between the stripes was 360°/80 = 4.5°. The stripes were set to 50% brightness. Stripes were present in all except the last epoch in both open- and closed-loop experiments. A circular band (elevation 65°, brightness 40%) was projected in all epochs to provide circularly symmetric illumination inside the dome. During the first 15 laps, before Epoch 1, a set of stationary landmarks—identical to those used in ref. 6—were superimposed over the stripes, and both stripes and landmarks were also stationary. Because this overlay of landmarks and stripes did not reliably provide strong cue control, likely because of the lack of visual salience of the landmarks against the striped background, this pre-Epoch-1 landmark condition was excluded from further analysis.

Training

Over 2–3 d, we familiarized the rats to human contact and trained them to wear a body harness (Coulbourn Instruments). The rats were placed on a controlled feeding schedule to reduce their weights to approximately 80% of their ad libitum weight, whereupon they were trained to run for a food reward (50% diluted Ensure®) on a training table in a different room from the experimental room. The training table had the same dimensions as the table inside the dome, but no enclosure or other automated systems. Reward droplets were manually placed at arbitrary locations on the track in the path of the running rat, and the experimenter attempted to lengthen the average interval between rewards to maintain behavior while delaying satiation. Training continued until the rats consistently ran 40 laps without intervention or encouragement from the experimenters. Training usually took 2–3 weeks.

Electrode implantation and adjustment

After training, rats underwent stereotactic surgery where they were implanted with hyperdrives containing 16 independently movable nichrome tetrodes, the tips of which were gold-plated to an impedance of ~150 kΩ using a nanoZ electroplating system (White Matter). The hyperdrives were fabricated in the laboratory using an in-house design and used a 72-channel interface board (EIB-72-QC, Neuralynx). Following surgery, 30 mg of tetracycline and 0.15 ml of a 22.7% solution of the antibiotic enrofloxacin were administered orally to the rats each day. After at least 4 d of recovery, we began slowly advancing the tetrodes and resumed food restriction and training within 7 d of surgery. Once the tetrodes were close to CA1, they were advanced less than 40 µm per day. The location of each tetrode relative to the CA1 pyramidal cell layer was judged using the polarity of sharp waves and intensity of ripples in the electroencephalogram (EEG) signal captured on one electrode of each tetrode, as per well-established procedures. Tetrodes were judged to be placed correctly when ripples were intense and multiple units were visible on the pairwise electrode projections of spike amplitudes.

Postsurgery training

During days of electrode advancement, we simultaneously food-restricted the rats. On (typically) day 3 of food restriction, we placed them into the Dome while wearing the body harness. A magnetic pad attached to the harness was used to mount a 6.4-mm marker (Optitrack) to track the position of the rat and actuate the enclosure surrounding the rat in real time, so that the rat remained near the center of the enclosure. To encourage movement in only one angular direction, the enclosure was never moved CW. Thus, as the rat approached the front (CCW end) of the enclosure, it moved forward. When the rat approached the back (CW end) of the enclosure, it did not move, thereby blocking the path of the rat. A pump dropped liquid reward in front of the running rat, which prompted the rat to move forward and thus move the enclosure. Reward was dropped at a spatial interval picked from a uniform distribution around a mean interval that varied across days depending on the rat's performance. Within a few days after surgery, rats learned to run continuously and obtain food reward. The mean interval of reward was gradually increased to maintain running performance until the presurgery performance criterion was reached once again (typically 7–10 d).

Neural recording

Once the tetrodes were judged to be in CA1 and the rat was again running at least 40 laps inside the dome, the experimental sessions began. During sessions, a unity-gain neural recording headstage (EIB-72-QC, Neuralynx) was attached to the implanted hyperdrive. The neural signals passed through a commutator and were filtered (600–6,000 Hz), digitized at 30 kHz and recorded on a computer running the Neuralynx Cheetah 5 recording software. Simultaneously, EEG data from one channel of each tetrode were filtered (1–475 Hz), digitized at 30 kHz and stored on the computer. Pulses sent from the experiment-control computer were time-stamped and recorded as events on the neural

recording computer to enable the post hoc synchronization of the data streams recorded on the two computers. Procedures for synchronizing and associating signals to the behavioral data are detailed in ref. 32. For experimental sessions, instead of the single large marker attached to the body harness, a set of smaller (3 mm, 4 mm) markers were placed in a rigid arrangement around the recording headstage. This allowed our custom algorithm to track the three-dimensional position and orientation of the constellation of markers with higher accuracy and robustness[62]. Thus, the rat did not need to wear the harness during sessions.

Experimental control

Three computers were used to run the experiment. Their purposes were: (1) general experiment control, (2) neural recording and (3) video tracking and neural recording. Multiple independent programs, called nodes, performed each of these tasks and communicated to a master node running on computer no. 1 and to each other through a software framework called Robot Operating System (ROS)[63]. Details on the hardware and software integration and experimental control are available in ref. 32.

Real-time firing rate computation

A python ROS node on the neural recording computer used the NetCom Application Programming Interface (API) to receive real-time neural data, and ROS APIs to receive tracked rat positions. Occupancy of the rat and spike counts from each tetrode were collected into 5° spatial bins covering a region six laps before the current angular position of the rat ($6 \times 360/5 = 432$ bins). Rat velocities were computed at 100 Hz, and a count was added to the current occupancy spatial bin if the velocity was above 5° s^{-1} (≈5 cm s^{-1}). Spikes from each tetrode were tested for high, correlated amplitudes (indicating noise) and then counted into their respective spatial bins if the current velocity was above threshold. Spike counts were divided by occupancy, and the resulting 432 firing rates (spikes per s) were made available at 1 Hz; no attempt was made to sort spikes generated by principal cells from those generated by interneurons. These firing rates were used by the online spectral decoder, described below, to decode hippocampal gain (Extended Data Fig. 1c) for each tetrode. Tetrodes that had no visible neurons or had noisy recordings were excluded by the experimenter using a manual interface, and the median of the gain estimates from the remaining tetrodes was termed the online hippocampal gain ($\hat{H}$) and used to manipulate stripe gain S during Epoch 2 of closed-loop sessions. The error between online gains $\hat{H}$ and H estimated post hoc using clustered units was low when $\hat{H}$ was used in the session (mean $|\hat{H} - H| < 0.1$ in Epoch 2 for 22 of 25 sessions, Extended Data Fig. 1d).

Spectral decoding

The algorithm for spectral decoding of hippocampal gain is detailed in Extended Data Fig. 1. The core algorithm remained the same as in our previous paper[6], but updates (described below) were made to improve the robustness of gain estimates. Briefly, we used the spatial periodicity of firing rates of place fields on a circular track to compute the spatial frequency of the population representation. For a stable spatial representation in the laboratory frame, a typical CA1 place cell would exhibit one firing field that repeats every lap, and hence the spatial frequency of firing is 1 cycle per lap. If a cell fired more (or less) than once per lap, its spatial frequency would be >1 (or <1) cycles per lap. The spatial frequency of firing is termed the hippocampal gain of each place cell.

In this version of the decoder, we improved the threshold mask used to enhance the signal-to-noise ratio of the spatial frequency content. The spatial spectrogram of the firing rate curve of each unit was first thresholded to the 80% percentile of its power in each spatial window. Contiguous regions above the percentile threshold were identified (MATLAB regionprops function). Noise regions tended to lack structure and agglomerated into punctate roundish blobs while the parts of the spectrogram denoting spatial frequency traces were larger in pixel count and more elongated. Given this, regions that were below a pixel area of 70,000 and an aspect ratio of 17 were removed from the mask. This thresholding mask was then applied to the sharpened spectrogram.

There were instances when the power in the fundamental trace failed to exceed the threshold described previously, causing the maximum-energy trajectory to follow a harmonic instead of the fundamental. An assumption was made that if the gain of a unit at a particular spatial window was a harmonic of another unit, the two units were likely from the same periodic signal. Harmonics were identified by taking the pairwise ratios between the gain estimates of all units at each spatial window. Ratios that were close to integer values indicated that the numerator was likely a harmonic of the denominator and were divided by this integer. These harmonic-corrected gain estimates from the individual units were binned in the space of unwrapped angular position and spatial frequency to identify if the set of gain estimates had a coherent grouping (all unit gain estimates fell within a 0.05 mean absolute error of each other) or if multiple subpopulations existed.

Offline decoding. The spectral decoder was run with a spatial window on each sorted unit passing inclusion criteria ('Data analysis', below). For each 5° spatial bin, the firing rate for each unit was calculated by dividing the number of spikes fired by that unit by the amount of time the rat spent in that bin when it was moving >5° s^{-1}. In accordance with standards in the field, this threshold corresponded to speeds at which theta power shows a marked increase[64] and was intended to remove spikes during the large irregular activity mode of hippocampal EEG, when place cell firing tends to be spatially nonlocal[65,66]. For each unit and for each bin, the hippocampal gain was the spatial frequency estimated by the spectral decoder on the 432 firing rates corresponding to the six-lap window before that bin. The population hippocampal gain H for each bin was computed as the median of these estimates across units.

Online decoding. During online decoding, the spectral decoder was run at 1 Hz on the 432 spatially binned firing rates for each tetrode corresponding to the six laps before the rat's current angular location. Thus, every second, a hippocampal gain estimate was generated for each tetrode. The population online hippocampal gain estimate $\hat{H}$ was the median of these estimates across the tetrodes chosen by the experimenter.

Mean gain ratio error. To evaluate the coherence of the recorded neural population, we quantified the deviation of the offline gain decoded from individual units to the population gain estimate. For each unit i and for each decoding window (six laps), the offline gain estimate H_i was compared against the population gain H, computed with H_i excluded. The gain ratio error was computed as $|1 - Hi/H|$ and the units were compared based on the mean of this value across all windows within a session (Fig. 2h and Extended Data Fig. 2).

Neurally closed-loop controller design

We hypothesized that we would be able to control the hippocampal gain H to a desired value by manipulating the stripe gain S during an experimental session, in response to an online decoded gain $\hat{H}$. Open-loop experiments demonstrated that changes in S produced changes in hippocampal gain H, but that this change effect is nonlinear. We made a reasonable approximation that

$$H_{\text{final}} - H_{\text{baseline}} = a + bS_{\text{final}}^{\text{m}}$$

Without stripe manipulation ($S_{\text{final}} = 1$), we do not expect H_{final} to deviate significantly from H_{baseline}. This was also subsequently supported by the data (paired t-test, H_{final} versus H_{baseline} in open-loop sessions where $S_{\text{final}} = 1$: $t(6) = -0.90$, $P = 0.40$). Thus, for the purpose of developing a feedback controller, we make the simplifying assumption that: $a = -b$. Open-loop data from rat 771 showed an exponent fit of

$m = 1.5$. For simplification of derivation, we further assumed a quadratic relationship ($m = 2$). These values were close to curve fits across rats in Fig. 2i (paired t-test, a versus $-b$: $t(4) = 1.92$, $P = 0.13$; m versus 2: $t(4) = 0.91$, $P = 0.41$). (Our failure to reject the null hypotheses in these low-sample datasets is used only to furnish a simplified model that is sufficiently expressive for neurally closed-loop control design, not to make definitive conclusions about the nature of the parameters.) Under these assumptions, we get the simplified model:

$$H_{\text{final}} - H_{\text{baseline}} = \frac{\kappa}{2}\left(S_{\text{final}}^2 - 1\right)$$

where $b = \frac{\kappa}{2}$. This corresponds to the integral equation:

$$\int_{H_{\text{baseline}}}^{H_{\text{final}}} \mathrm{d}H = \kappa \int_{1}^{S_{\text{final}}} S\mathrm{d}S$$

Ignoring constants of integration, the model relating the change in stripe gain dS to the hippocampal gain dH is thus

$$dH = \kappa S\, dS$$

At the initial value of $S = 1$, the linearized system dynamics is given by $\mathrm{d}H = \kappa\, \mathrm{d}S$. We designed a controller for this simplified system that reduces the error between the decoded gain $\hat{H}$ and the desired value H_{desired}. In scenarios where a control input (S) is used to drive a system state (H) to a desired state H_{desired}, a proportional controller could be used. For such a controller, the input is proportional to the error between $\hat{H}$ and H_{desired}.

$$S = K_P(H_{\text{desired}} - \hat{H})$$

In our case, at a particular $\hat{H}$ and H_{desired}, the error would remain constant, and thus S will be constant. Thus, d$S = 0$, which means that d$H = 0$ as well. Moreover, proportional control can require large gains to reduce the error, and large gains would lead to rapid changes in stripe movement such that the virtual environment may no longer have appeared to be stable to the animal. Due to these reasons, we chose an integral controller, known to be able to eliminate steady-state errors under appropriate conditions:

$$S = K_I \int_{\theta_0}^{\theta} (H_{\text{desired}} - \hat{H})\mathrm{d}\vartheta$$

The integration is initiated at $S_0 = 1$ in our case (the value of the stripe gain at the beginning of Epoch 2). The term K_I is the 'integral gain' (terminology from control theory, not to be confused with other 'gains' in the manuscript), and θ is the angle of the rat on the table. As a practical matter, the gain S produced by the integral controller was not allowed to go below 0.1 or above 4.0; these limits were reached in only 5 of 25 sessions (4 sessions saturated at 0.1, and 1 session at 4.0).

The block diagram of the feedback system consisting of the rat and controller is shown in Extended Data Fig. 7. The feedback loop consists of the controlled 'plant' P (in this case, the hippocampal circuit), the integral controller C and the feedback, which is our decoder, represented by a moving average over a window of six laps. We performed a Nyquist stability analysis to determine the range of integral gain K_I over which the controller would be stable. When the frequency of the input signal $s = j\omega$ is swept from 0 to ∞, if the loop gain L intersects the real axis at a point less than −1, the system would be unstable. To determine this point:

$$L = CP\frac{(1 - e^{-6s})}{6s} = \kappa\frac{K_I}{s}\frac{(1 - e^{-6s})}{6s} = -\kappa\frac{K_I}{6\omega^2}(1 - \cos(6\omega) + \mathrm{j}\sin(6\omega))$$

Here, $\mathrm{j} = \sqrt{-1}$. Setting $\mathrm{Im}[L] = 0$ (where Im[.] refers to the imaginary component of a complex number), the first point of intersection with the real axis is at $\omega = \frac{\pi}{12}$.

The intersection with the real axis is $\mathrm{Re}\left[L\left(\omega = \frac{\pi}{12}\right)\right] = -\frac{24K_I\kappa}{\pi^2}$ (where Re[.] refers to the real component of a complex number). To maintain stability, this intersection point needs to be to the right of −1, requiring $K_I < \frac{\pi^2}{24\kappa}$. According to our fitted power law (Fig. 2i), $b = 0.2$, and thus $\kappa = 0.4$; hence the condition for stability is $K_I < 1.03$. We used $K_I = 0.2$ in our closed-loop sessions, staying well within this margin of stability.

Stripe gain selection and ramp rates

In open-loop sessions, rats ran 15 laps with stripes on and stationary (Epoch 1; Fig. 2a,c,e). In Epoch 2, S was increased or decreased to S_{final}. The values of S_{final} were chosen to be of the form $1 \pm n/13$, with $n = 2, 6, 10$, resulting in gains of 0.231, 0.539, 0.846, 1.154, 1.462 and 1.769. These values with a prime denominator were chosen to reduce ambiguity between frames and ensured that during Epoch 3 the position of the rat relative to the laboratory and stripe frames of reference aligned only once every 13 laps. Gains were changed at a constant rate of 1/52 per lap, such that the length of Epoch 2 was 8, 24 and 40 laps for $n = 2$, 6 and 10, respectively. The sessions were not randomized; the gain for each session was selected such that gains were rarely repeated in consecutive sessions, and the gain manipulation typically increased in magnitude over consecutive sessions for any given animal. The investigators were not blinded to allocation during experiments and outcome assessment. No statistical methods were used to predetermine sample size.

In closed-loop sessions, Epoch 1 was identical to open-loop sessions. The hippocampal gain decoder was initialized and the gain estimate $\hat{H}$ was monitored during Epoch 1, but not used for cue manipulation. H_{desired} was either specified before the session, in which case it was chosen from the aforementioned values of the form $1 \pm n/13$, or it was set to be a constant offset of ±0.25 or ±0.5 from the estimated value of H_{baseline}. In either case, the H_{desired} value was set and not modified once the controller was initialized at the beginning of Epoch 2.

Data analysis

Spike sorting. For each triggered spike waveform, features such as peak, valley and energy were used to sort spikes using a custom software program (WinClust; J.J.K.). Cluster boundaries were drawn manually on two-dimensional projections of these features from two different electrodes of a tetrode. We mostly used maximum peak and energy as features of choice; however, other features were used when they were required to isolate clusters from one another. Clusters were assigned isolation quality scores ranging from 1 (very well isolated) to 5 (poorly isolated), agnostic to their spatial firing properties. Only clusters rated 1–4 were used for quantitative analyses including offline estimation of hippocampal gain.

Inclusion criteria. To be included in the quantitative analyses, sessions were required to meet the following criteria: sessions with stripe manipulation must have been run all the way to completion, that is, the rat finished the session (Epochs 1–3, and removed after stripes were extinguished), and there were no major behavioral issues or long manual interventions during the session, as per our experimental notes. Session inclusion was determined before performing any of the statistical analyses across sessions detailed in this manuscript. For the 65 sessions that met these criteria, spikes that occurred when the movement speed of the rat was less than 5° s^{-1} (about 5 cm s^{-1}) were removed. Units were required to fire at least 50 spikes during the session to be included. Interspike interval (ISI) for a unit was computed as the peak of the histogram of difference in spike times. Units were categorized as putative principal cells or interneurons based on a k-means clustering algorithm with firing rate, spike width and ISI as dimensions[67]. Units formed two clusters: consistent with well-established standards, pyramidal cells fired at lower rate, had broader spikes and had larger ISI than interneurons. Both putative principal cells and interneurons were included in the offline estimation, as segregation of units into

putative principal cells and interneurons did not affect the results (Extended Data Fig. 2).

Closed-loop control categorization. We categorized closed-loop control sessions based on the value of the hippocampal gain at the end of Epoch 2, H_{final}, in comparison with the desired gain, $H_{desired}$, as follows: controlled if $|H_{desired} - H_{final}| < 0.05$, moderately controlled if $0.05 \leq |H_{desired} - H_{final}| < 0.20$ and uncontrolled if $|H_{desired} - H_{final}| \geq 0.20$. The thresholds of 0.05 and 0.20 were chosen subjectively based on visual inspection of the graphs in Extended Data Fig. 8.

Histology

Once experimental sessions were complete, rats were transcardially perfused with 3.7% formalin. The brain was extracted and stored in 30% sucrose–formalin solution until fully submerged. For four rats, the brain was sectioned coronally at 40-µm intervals. The sections were mounted and stained with 0.1% Cresyl violet, and each section was photographed. These images were used to identify tetrode tracks, on the basis of the known tetrode bundle configuration. A depth reconstruction of the tetrode track was carried out for each recording session to identify the specific areas in which the units were recorded. For one rat, we optically cleared the whole brain using the AdipoClear+ protocol[68]. The cleared brain was imaged using a lightsheet microscope (Ultramicroscope, LaVision BioTec) and the tetrode tracks were visualized in the autofluorescence channel using Imaris software to identify areas where units were recorded.

Statistics

No statistical methods were used to predetermine sample sizes but our sample sizes are similar to those reported in previous publications[6,12,13,43,65]. Parametric tests were used to determine statistical significance. Pearson product–moment correlations were used to test the linear relationship between variables. For nonlinear relationships, data were fit using nonlinear least-squares (MATLAB fit function) with specified model structures and goodness-of-fit statistics (residual d.f. = $n - m$, where n is number of data points and m is number of parameters, as well as d.f.-adjusted coefficient of determination (R^2) are reported). Paired, two-sided t-tests were used to compare information scores in laboratory, stripe and hippocampal frames of reference. Data distribution was assumed to be normal but this was not formally tested. To prevent sampling the same cells across days for this analysis, the experimental session with the greatest number of units was chosen for each rat and for each tetrode. Mean and s.e.m. were used to plot information scores across units. LMEs were used to test the significance of recalibration across all animals, with $(H_{recal} - H_{baseline})$ as the dependent variable, $(H_{final} - H_{baseline})$ as a fixed-effect independent variable and rat identity as a random-effect dependent variable. The model was fit using the command fitlme in MATLAB. A separate LME was also run with S_{final} as the fixed-effect dependent variable, to test whether S_{final} or $(H_{final} - H_{baseline})$ was a better predictor of $(H_{recal} - H_{baseline})$. We used the criterion of a difference in BIC > 6 to indicate a meaningful difference between the two models[52].

Simulation of biased drift in path integration

To simulate the drift in path integration gain, we modeled it as an iterative loop between two processes. First, a noisy stripe gain signal S influences the hippocampal gain using the optic flow response model fit in Fig. 2i, moving it from a baseline value $H_{baseline}$ to H_{final}.

$$H^{t}_{final} - H^{t}_{baseline} = a + b(S^{t})^{m} \quad (1)$$

Then, following the linear fit quantifying recalibration in Figs. 3c and 5c, a portion of the change in hippocampal gain is remembered due to recalibration and alters $H_{baseline}$ in the next iteration. These processes can be written out for step t as follows:

$$H^{t+1}_{baseline} - H^{t}_{baseline} = k(H^{t}_{final} - H^{t}_{baseline}) \quad (2)$$

Substituting (1) into (2) and iterating gives:

$$H^{t+1}_{baseline} = H^{0}_{baseline} + k\sum_{k=0}^{t}(a + b(S^{k})^{m}) \quad (3)$$

Initial baseline value $H^{0}_{baseline}$ is assumed to be 1. Parameters were chosen within the confidence intervals of the data fits (Fig. 2i; slope coefficient in LMEs): $b = 0.2$; $a = -b$; $m = 2$; $k = 0.3$. The stripe gain S was assumed to be a constant input at unity with independent and identically distributed uniform random noise ε (±0.25 interval) added to it at each iteration, that is, $S^{k} = 1 + \varepsilon$.

Equation (3) was iterated across spatial increments of approximately 50° for a length of 15 laps (duration of Epoch 1 in open-loop sessions). This constituted one 'run' of the simulation. The slope of the drift in gain over the 15 laps was computed. The histogram of the slopes from 10,000 runs is shown in Extended Data Fig. 4c.

Reporting summary

Further information on research design is available in the Nature Portfolio Reporting Summary linked to this article.

Data availability

Preprocessed data used to perform the analyses and generate the figures in this manuscript are available in the Johns Hopkins Research Data Repository, at https://doi.org/10.7281/T1/THLC8N.

Code availability

Custom code was written to analyze the datasets used in this study, and to generate figures for this manuscript. This codebase is versioned, and uses several third-party packages, the license files for which are included with the respective code. The codes used to perform the analyses and generate the figures in this manuscript are available in the Johns Hopkins Research Data Repository, at https://doi.org/10.7281/T1/THLC8N.

References

62. Vagvolgyi, B. P., Jayakumar, R. P., Madhav, M. S., Knierim, J. J. & Cowan, N. J. Wide-angle, monocular head tracking using passive markers. *J. Neurosci. Methods* **368**, 109453 (2022).
63. Quigley, M. et al. ROS: an open-source robot operating system. in *ICRA Workshop on Open Source Software* vol. 3 p. 5 (IEEE, 2009).
64. Kennedy, J. P. et al. A direct comparison of theta power and frequency to speed and acceleration. *J. Neurosci.* **42**, 4326–4341 (2022).
65. Pfeiffer, B. E. & Foster, D. J. Hippocampal place-cell sequences depict future paths to remembered goals. *Nature* **497**, 74–79 (2013).
66. Jeewajee, A., Barry, C., O'Keefe, J. & Burgess, N. Grid cells and theta as oscillatory interference: electrophysiological data from freely moving rats. *Hippocampus* **18**, 1175–1185 (2008).
67. Csicsvari, J., Hirase, H., Czurkó, A., Mamiya, A. & Buzsáki, G. Oscillatory coupling of hippocampal pyramidal cells and interneurons in the behaving Rat. *J. Neurosci.* **19**, 274–287 (1999).
68. Branch, A. et al. An optimized tissue clearing protocol for rat brain labeling, imaging, and high throughput analysis. Preprint at *bioRxiv* https://doi.org/10.1101/639674 (2019).

Acknowledgements

We thank E. Fortune for providing valuable comments on the manuscript; K. Nnah, A. Branch, M. Ferreyros, B. Krishnan, B. Vagvolgyi and V. Puliyadi for technical assistance; and H. T. Blair for useful discussions. This work was supported by US Public Health Service grant no. R01 NS102537 (N.J.C., J.J.K., F.S.) from the NINDS,

a Johns Hopkins University Kavli Neuroscience Discovery Institute Distinguished Postdoctoral Fellowship (M.S.M.), a Johns Hopkins University Provost's Undergraduate Research Award (B.Y.L.), ARO Grants no. W911NF1810327 (N.J.C., J.J.K.) and a Discovery Award from the Johns Hopkins University (N.J.C., J.J.K.).

Author contributions

M.S.M., R.P.J., F.S., J.J.K. and N.J.C. conceived and designed the study. J.J.K. and N.J.C. supervised all aspects of the experiments and analysis. R.P.J. and M.S.M. designed and constructed the apparatus, performed experiments and analyzed the data. B.Y.L. performed experiments and analyzed data. S.G.L. and K.W. performed experiments. M.S.M., R.P.J., B.Y.L., J.J.K. and N.J.C. wrote the paper and F.S. and S.G.L. provided critical feedback.

Competing interests

The authors declare no competing interests.

Additional information

Extended data is available for this paper at https://doi.org/10.1038/s41593-024-01681-9.

Supplementary information The online version contains supplementary material available at https://doi.org/10.1038/s41593-024-01681-9.

Correspondence and requests for materials should be addressed to Manu S. Madhav, James J. Knierim or Noah J. Cowan.

Peer review information *Nature Neuroscience* thanks Loren Frank, Edvard Moser, Aman Saleem and the other, anonymous, reviewer(s) for their contribution to the peer review of this work.

https://doi.org/10.1038/s41593-024-01681-9

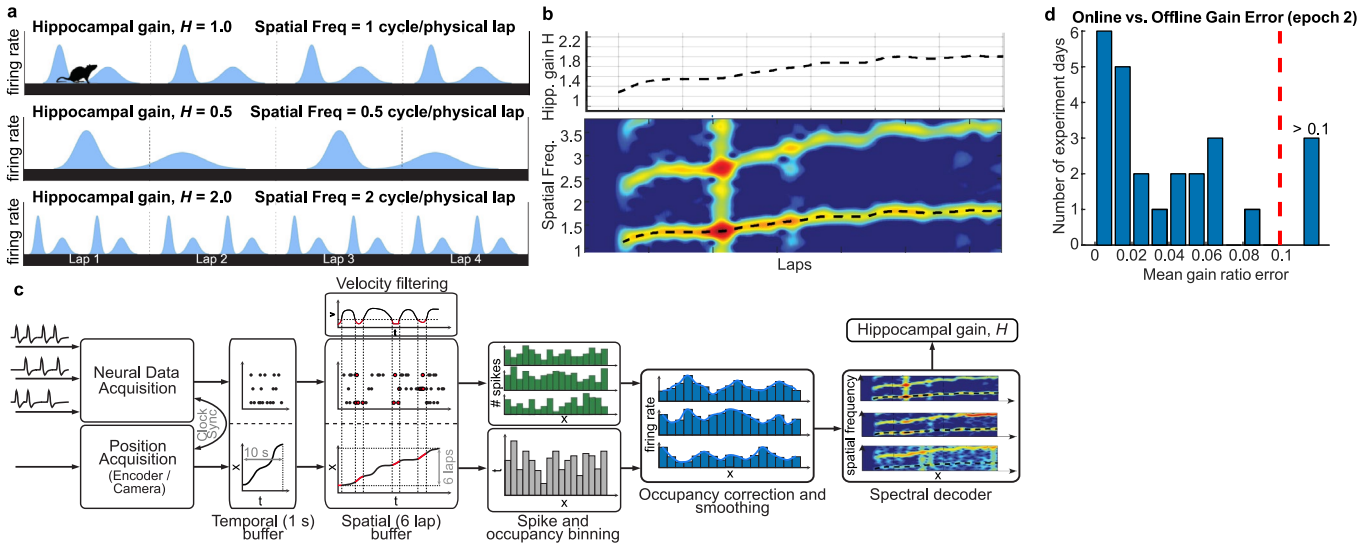

Extended Data Fig. 1 | Hippocampal gain decoding. (a) If a unit has a characteristic spatial tuning that repeats once per physical lap, the firing rate of the unit exhibits a spatial frequency of $H = 1$ per lap. Illustration of the firing of a spatially tuned cell for three values of hippocampal gain, H. **(b)** Reproduction of data from Fig. 1d, f. The spectrogram of one unit is shown at the bottom, with the color denoting the power at a given position and spatial frequency. Spectrogram peaks emerge at a fundamental frequency starting at ~1.1 and at its harmonics. We use a custom algorithm to trace these peaks (see 'Spectral Decoding' in Methods) and estimate the gain for each unit. The hippocampal gain, H, is estimated as the median spatial frequency across all isolated units for a given session. **(c)** Real-time decoding flowchart. Neural data from each tetrode and rat position data from the camera are acquired (see[62] for hardware details). Incoming spike times, as detected by Neuralynx spike detection parameters, and positions are added to a temporal buffer. The following operations are performed every 1 s. The temporal buffer is transferred into a spatial queue buffer that accumulates spike times and positions from the previous 6 laps. Velocities are computed from positions, and spikes and positions with velocities <5 cm/s are eliminated. The remaining spikes and positions are spatially binned (5° width). The spike bins are divided by position bins to create firing rate bins for each tetrode, which are then smoothed and sent to the spectral decoder to estimate H (details in Methods section and Fig. 1d–g). The spectral decoder is able to estimate spatial frequency from the cumulative spatial tuning of all simultaneously recorded cells on a tetrode, extending the success of decoding spatial frequency from cells with such diffuse spatial tuning like interneurons (described in[6]). Spatial frequencies estimated independently from each tetrode were combined together into $\hat{H}$, to be robust to noisy estimates on any particular tetrode. **(d)** Comparison of online (unsorted) decoding vs. offline (sorted) decoding in Epoch 2 (controller on and using online decoded values) of the 25 closed-loop sessions. The mean absolute error between these gains remains close to 0, with a few sessions (3/25) showing deviations greater than 0.1.

https://doi.org/10.1038/s41593-024-01681-9

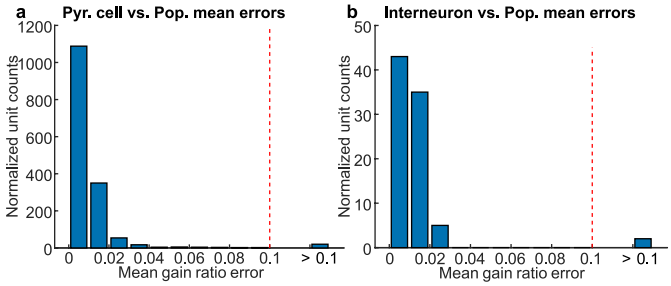

Extended Data Fig. 2 | Comparison of population coherence of putative pyramidal cells and interneurons. Here, the data from Fig. 2h is split into **(a)** putative pyramidal cells (1549 units) and **(b)** putative interneurons (85 units) that were identified in all data (see Methods). If a unit, *i*, were part of a coherent population, its gain *Hi* should equal the population hippocampal gain *H*. For each 6-lap window we computed a gain ratio error $|1-Hi/H|$ and computed the average of this value across the session to derive the coherence score for the unit. To avoid bias, for each unit *i*, H_i was excluded from the computation of population gain *H*. Most units in both populations have a score very close to zero and very few have values above 0.1 (19/1549 pyramidal, 2/85 interneurons). These populations were thus combined in the other analyses.

https://doi.org/10.1038/s41593-024-01681-9

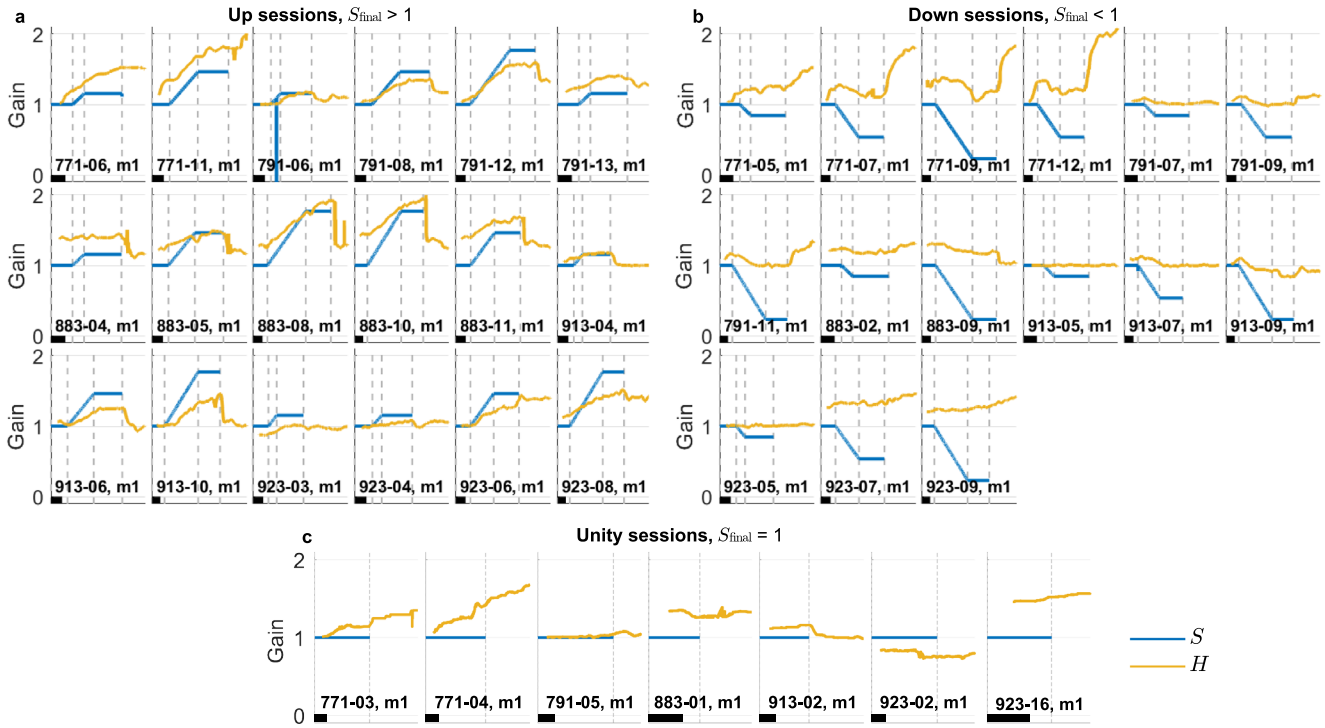

Extended Data Fig. 3 | Gain dynamics during all open-loop sessions. Gain dynamics during all open-loop sessions (including sessions illustrated in main text figures). Each plot represents a single session (titled as 'Rat-Day, Session', 40 sessions across 5 rats). X axis is number of laps the rat ran on the table and Y axis is gain. The black scale bar in each plot denotes 10 laps. Applied stripe gain (*S*; blue) plotted with decoded hippocampal gain (H; yellow). Sessions are grouped by the final stripe gain: **(a)** Up sessions ($S_{final} > 1$), **(b)** Down sessions ($S_{final} < 1$), and **(c)** Unity sessions ($S_{final} = 1$). Dashed vertical lines indicate boundaries between Epochs 1, 2a, 2b and 3 for Up and Down sessions, and between Epochs 1 and 3 for Unity sessions. The blips in the *S* curve in session 791–06, m1 was the result of a momentary software error. In most of the Up sessions, the hippocampal gain increases at a faster rate in Epoch 2a (*S* ramps up) than in Epoch 1 ($S = 1$). In many Down sessions, the hippocampal gain appears to decrease slowly, stay stable, and or even increase over laps, even though the stripe gain is decreasing. This may be the result of two effects—high baseline and low influence of stripes when gain is changed in the downward direction. In general, reducing the stripe gain has a lower influence on H than increasing the gain (Fig. 2i). These two factors combine: in the first four sessions of panel b, H rises up to $H_{baseline}$ in Epoch 1, but this upward drift is arrested and overcome by larger decreases in S (panel b, sessions 2, 3, and 4) but not quite overcome by a smaller decrease in S (panel b, session 1). For one animal (883), we observed a 'rebound' in the hippocampal gain after the stripes were extinguished, resulting in a consistent offset (that is, a negative intercept and low slope in the recalibration line, Fig. 3c, yellow); despite this offset, there was still a linear relationship between $H_{final} - H_{baseline}$ and $H_{recal} - H_{baseline}$ for each rat (Fig. 3c), demonstrating the recalibration phenomenon.

https://doi.org/10.1038/s41593-024-01681-9

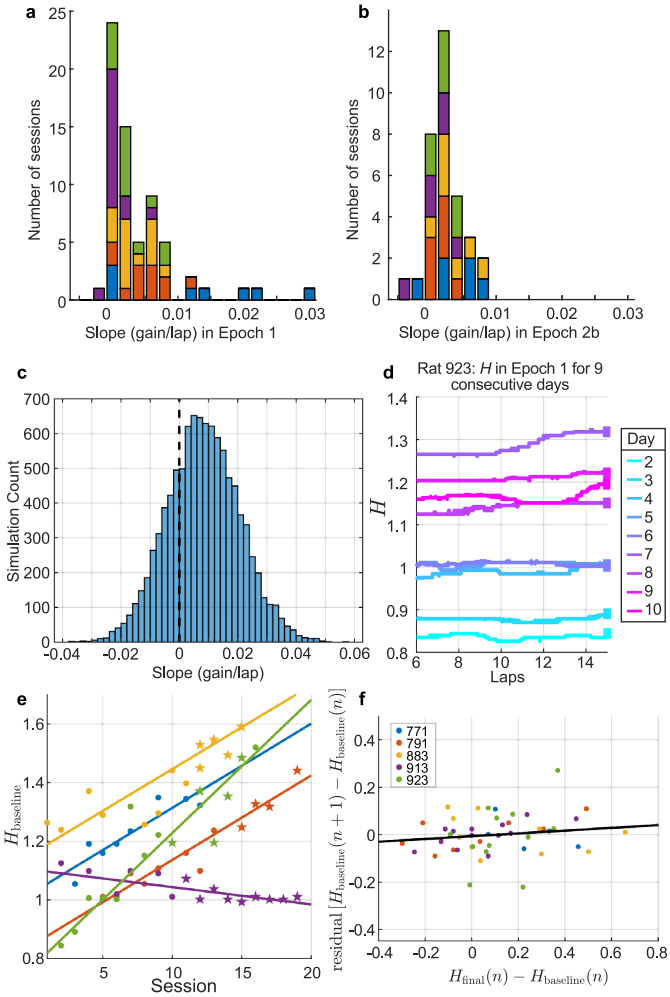

Extended Data Fig. 4 | Hippocampal gain drift. (a) Data from Epoch 1 of all open and closed-loop sessions where the stripe gain was held at 1. Most sessions have a positive slope. **(b)** Data from Epoch 2b of open-loop sessions where the stripe gain was held constant for 26 laps at a value not equal to 1. Most sessions have a positive slope. The *x* axis shows slopes of the linear fits of the hippocampal gain in these respective epochs and the *y* axis shows the session count. Colors indicate individual animals (see key in (f)). **(c)** Simulation of drift in path integration gain within session. We created a simulation to test the hypothesis that the positive drift might be caused by the asymmetric responses of the hippocampal gain to UP and DOWN manipulations of stripe gain (Fig. 2i, Extended Data Fig. 4a, b). Under the assumption that the velocity inputs are noisy, the asymmetric response would result in any noise deviation in the UP direction having a stronger influence on the updating of position on the hippocampal map than noise deviations in the DOWN direction. If the gain is continually recalibrated, the biased influence of noise and gain recalibration results in a biased random walk toward higher gain values (description in Simulation of biased drift in path integration under Methods). An iterative model was fed a noisy stationary optic flow gain input for 15 laps. As predicted, the output hippocampal gain exhibited a biased drift toward higher gain values. The *x* axis shows slopes of the linear fits of the hippocampal gain in these 15 laps and the *y* axis shows the run count for each slope bin. (An alternative explanation reverses the causal relationship between the observed asymmetry and the observed drift. That is, the asymmetry might result from a biased drift inherent in the system, which would need to be counteracted to drive the hippocampal gain down in the DOWN condition. In contrast, this bias would presumably augment the effects of increasing optic flow gain in the UP condition. We currently cannot distinguish between these two possible explanations of the relationship between biased drift and asymmetrical influence of optic flow.) **(d)** Example of baseline shift across days in one rat. The *y* axis is hippocampal gain, *H*, during the first 12 laps of Epoch 1 (stripes stationary) for 9 consecutive sessions. The last point in each curve (square marker) is considered H_{baseline} for the session. The *x* axis denotes laps on the table. For Rat 923, the value of H_{baseline} steadily increased across sessions but was relatively stable within a session. **(e)** Baseline shifts across sessions (typically 1 session/day) for individual rats. Data from each rat is plotted in a different color. The *x* axis is the session number of each rat and the *y* axis is H_{baseline} for that session. Dots denote open-loop sessions and stars denote closed-loop sessions. 4/5 rats show a significant positive drift of H_{baseline} over sessions (Rats= 771,791,883,923: slope = 0.029, 0.029, 0.029, 0.049; r^2 = 0.82, 0.93, 0.73, 0.91; two-sided t-test against null hypothesis of slope 0, t-statistic = 5.18, 11.5, 5.88, 11.1, $p = 2.05 \times 10^{-3}$, 4.47×10^{-7}, 5.37×10^{-5}, 1.13×10^{-7}; n = 8, 12, 15, 14 ; df = 6, 10, 13, 12, no adjustment made for multiple comparisons) whereas one rat showed a significant negative drift (Rat 913: slope = −0.006, r^2 = 0.44; two-sided t-test, t-statistic = −3.33, $p = 4.98 \times 10^{-3}$; n = 16, df = 14). Because of these shifts, we subtracted H_{baseline} from the dependent measures in our analyses of Figs. 2g, 3c, 4h, and 5c. We speculate that the baseline shift across days, shown in panels (d) and (e), may be due to an accumulation of within-session biased drift shown in (a) and (b) and simulated in (c). Future work exploring the question of biased drift may help explain observed behavioral path integration error biases[49,50]. **(f)** While there was an overall linear trend in the baseline over all sessions (panel e), it is unclear if, on a day-to-day basis, the baseline shift was influenced by the effect on *H* from the previous session's manipulation. Typically, we alternated up and down manipulations in successive sessions, so if there were such a day-to-day influence, the residual around the linear trend should be correlated with the magnitude of the previous day's manipulation. To examine if there was a systematic influence of the previous session's manipulation on this residual, we plotted the residual (that is, the change in the baseline on session (n + 1), minus the linear trend from (e)) versus the gain change induced by stripes on the previous session, $H_{\text{final}}(n) - H_{\text{baseline}}(n)$. There was no significant relationship between these variables (r^2 = 0.02, two-sided t-test, t-statistic = 1.07, p = 0.29, n = 48, df = 46).

https://doi.org/10.1038/s41593-024-01681-9

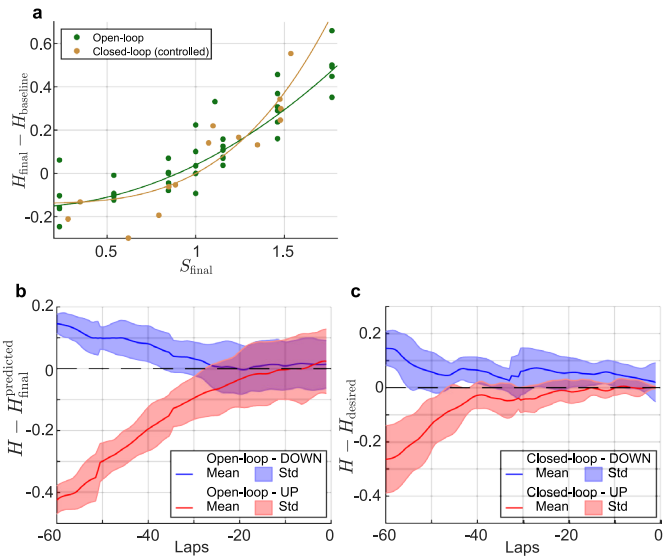

Extended Data Fig. 5 | Comparison of open-loop and closed-loop control. **(a)** As might be expected, regardless of the control scheme implemented, the nonlinear relationship between change of hippocampal gain from its Epoch 1 baseline value (y-axis) and stripe manipulation (x-axis) is similar in open-loop (green fit) and closed-loop (orange fit) sessions. **(b-c)** The utility of closed-loop control is to drive the hippocampus to a desired state and hold it there. To demonstrate its effectiveness in this regard, we compared it with how well an open-loop experiment would perform. **(b)** Neurally open-loop (feedforward) control: The nonlinearity described in panel (a) can be used to predict H_{final} for a given open-loop stripe manipulation, S_{final}. However, rather than using all of the data to fit the model as in panel (a), an individual model fit was made for each open-loop session using the remaining open-loop sessions (leave-one-out). The y-axis shows a 1-lap moving average of the difference between the measured hippocampal gain, H, and the predicted gain from the leave-one-out fit for that session, $H^{predicted}_{final}$, in the laps (x-axis) leading up to the stripes being turned off (zero point on x-axis). The stripe gain was held at S_{final} for 26 laps prior to the stripes being turned off. Data are shown as mean ± standard deviation, with the dark lines representing mean and shaded region representing standard deviation. DOWN sessions ($S_{final} < 1$) are shown in blue and UP sessions ($S_{final} > 1$) are shown in red. The means of both UP and DOWN sessions approached close to zero offset from the predicted value, albeit with a large standard deviation. **(c)** Neurally closed-loop (feedback) control: in strongly and modestly controlled neurally closed-loop sessions, a target state, $H_{desired}$, was defined prior to each session. The controller was able to achieve close to zero-offset in both UP ($H_{desired} > H_{baseline}$) and DOWN ($H_{desired} < H_{baseline}$) sessions, but with notably lower standard deviations than in panel (b), demonstrating tighter control of H for neurally closed loop sessions compared to neurally open loop sessions.

https://doi.org/10.1038/s41593-024-01681-9

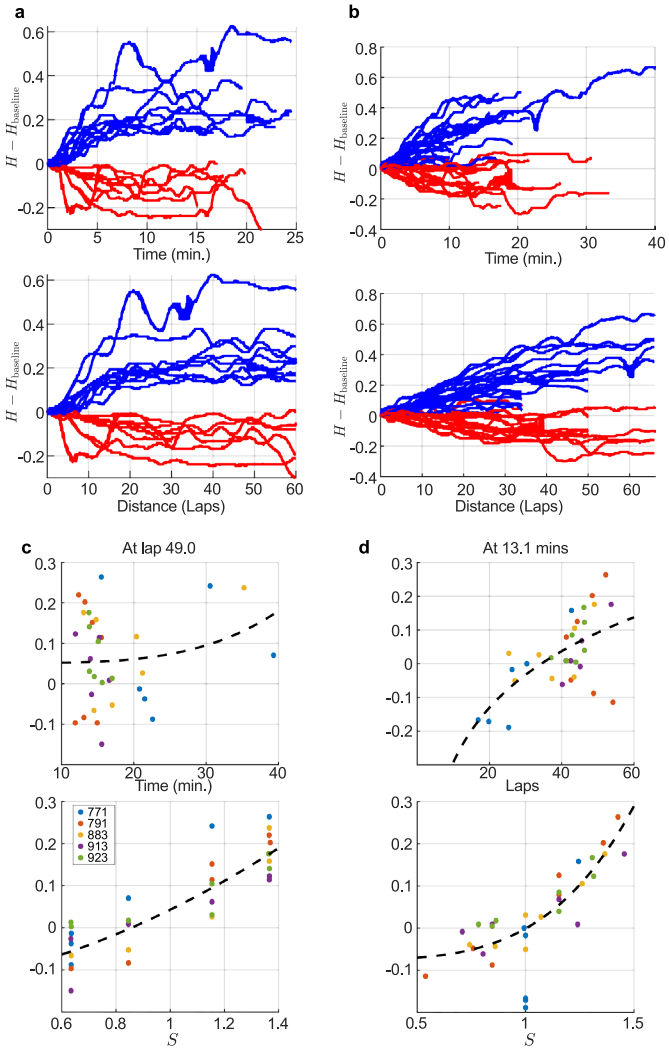

Extended Data Fig. 6 | Examining time and distance confounds. Because our manipulations generally require gradually increasing (or decreasing) gain in a monotonic fashion, it was necessary to ensure that the concomitant increase in time and distance were not confounding, critical factors that determined the evolution of the hippocampal gain. **(a, b)** Evolution of $H–H_{baseline}$ in Epoch 2 for **(a)** controlled closed-loop sessions for which the target gain was away from 1 and **(b)** open-loop sessions such that S_{final} was away from 1, plotted as a function of time (top) and distance run (bottom). In closed-loop sessions, the controller moved H either up ($H_{desired} > H_{baseline}$, blue, 10 sessions) or down ($H_{desired} < H_{baseline}$, red, 9 sessions). In open-loop sessions, the stripe gain was either increased ($S_{final} > 1$, blue, X sessions) or decreased ($S_{final} < 1$, red, X sessions). Time and distance only increase (+) in these experiments but the hippocampal gain followed the sign of the manipulation, clearly indicating the strong causal control of our stripe manipulations above any potential confounding influence of time or distance. **(c, d)** We also examined the influences of distance run and time spent under stripe manipulation to the change in hippocampal gain, $H–H_{baseline}$, compared to our stripe gain manipulation S. These analyses were run for all open-loop sessions where $S_{final} \neq 1$. **(c)** For these sessions, we computed the minimum distance rats ran in Epoch 1 and 2 (49 laps, the distance run in the $S_{final} = 1 \pm 2/13$ sessions) to equate distance across gain manipulations. At 49 laps after the start of Epoch 1, the change in hippocampal gain $H–H_{baseline}$ is plotted as a function of both time (top) and stripe gain S (bottom) for all sessions. Each data point is from a session and colors denote different rats. We fit a power-law curve to both plots ($H–H_{baseline} = a + bx^m$). There is no obvious relationship between $H–H_{baseline}$ and time (adjusted $r^2 = -0.26$, $df = 30$), whereas there is a power-law relationship to S (adjusted $r^2 = 0.69$, $df = 30$) similar to Fig. 2i. **(d)** For these sessions, we computed the minimum time rats ran in Epochs 1 and 2 (range 13.1–19.9 mins). At 13.1 mins after the start of Epoch 1, the change in hippocampal gain $H–H_{baseline}$ is plotted as a function of both distance run (top) and stripe gain S (bottom). There is no strong relationship between $H–H_{baseline}$ and distance (adjusted $r^2 = -0.077$, $df = 30$) whereas there is a clear power-law relationship to S (adjusted $r^2 = 0.72$, $df = 30$), similar to Fig. 2i. From these plots, we conclude that the change in H in these experiments is related to S and not to the correlated variables, time and distance travelled.

https://doi.org/10.1038/s41593-024-01681-9

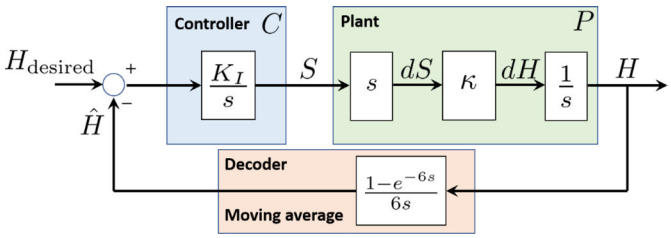

Extended Data Fig. 7 | Block diagram of closed-loop controller. Here, s is the Laplace complex frequency variable. Multiplication by s denotes differentiation, whereas dividing by s denotes integration. C is the implementation of our neurally closed-loop controller, namely the transformation from the error ($H_{\text{desired}} - \hat{H}$) to the stripe gain S. In control theoretic terminology, the controlled system (hippocampal circuit) is the 'plant' P, which transforms the stripe gain S into the output H. The term $\frac{(1-e^{-6s})}{6s}$ in the feedback loop is the transfer function of a 6-lap moving average, capturing the lag introduced by our online gain decoder. The transfer function of the controller is $C = \frac{K_I}{s}$ and that of the plant reduces to a constant gain, $P = \kappa$.

https://doi.org/10.1038/s41593-024-01681-9

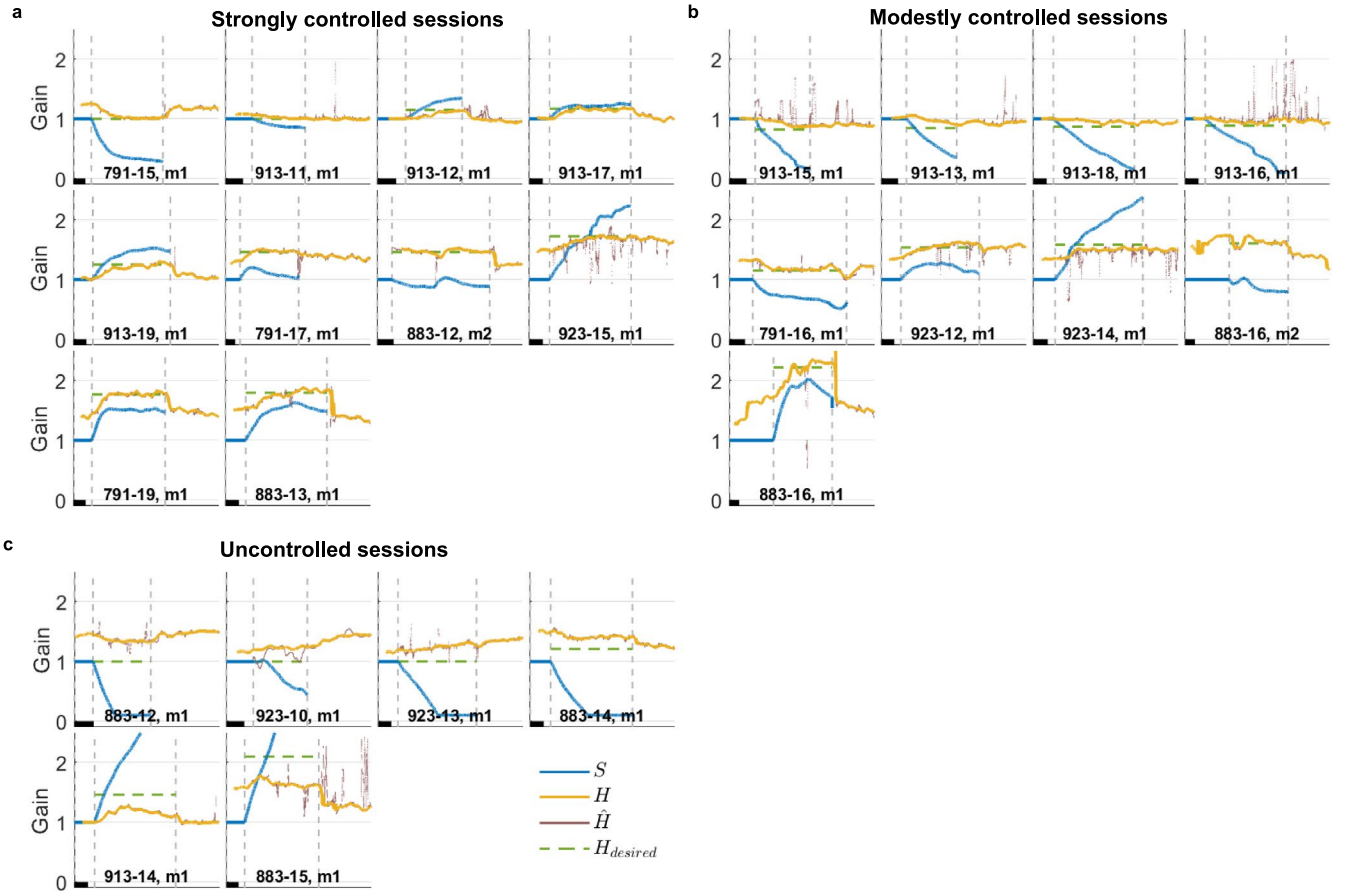

Extended Data Fig. 8 | Gain dynamics during all closed-loop sessions. Gain dynamics during all closed-loop sessions (including sessions illustrated in main text figures). Each plot represents a single session (titled as 'Rat-Day, Session', 25 sessions across 4 rats). X axis is laps the rat ran on the table and Y axis is gain. The black scale bar in each plot denotes 10 laps. Applied stripe gain (S; blue) plotted with offline-decoded hippocampal gain (H; yellow) and hippocampal gain estimated online using unsorted spikes ($\hat{H}$; brown). This estimated value was driven to a constant desired value during the session ($H_{desired}$; green dashed line). Dashed vertical lines indicate boundaries between Epochs 1, 2 and 3. Data is sorted into three groups based on how closely the final hippocampal gain (H_{final}) matched $H_{desired}$ (see Methods): **(a)** strongly controlled sessions ($|H_{final} - H_{desired}| < 0.05$), **(b)** modestly controlled sessions ($0.05 \leq |H_{final} - H_{desired}| < 0.20$), and **(c)** uncontrolled sessions ($|H_{final} - H_{desired}| \geq 0.20$). Note that $\hat{H}$ is a real-time estimate that depended on neural noise inherent in multi-unit electrophysiology and varied in quality day-to-day. $\hat{H}$ was utilized only in Epoch 2 and even then, our slow-moving integral controller mitigated the effects of momentary noise in the estimate. For sessions in which $H_{desired} > 1$ (Up sessions), 8 were strongly controlled, 5 were moderately controlled, and 3 were uncontrolled. For sessions in which $H_{desired} \leq 1$ (Down sessions), 2 were strongly controlled, 4 were moderately controlled, and 2 were uncontrolled. The small numbers of sessions do not provide enough power for statistical testing, but the apparent differences in closed-loop control between Up and Down sessions is discussed in the main text.

nature portfolio

Corresponding author(s): Manu S. Madhav, Noah J. Cowan

Last updated by author(s): 2024-03-27

Reporting Summary

Nature Portfolio wishes to improve the reproducibility of the work that we publish. This form provides structure for consistency and transparency in reporting. For further information on Nature Portfolio policies, see our Editorial Policies and the Editorial Policy Checklist.

Statistics

For all statistical analyses, confirm that the following items are present in the figure legend, table legend, main text, or Methods section.

n/a	Confirmed	
☐	☒	The exact sample size (*n*) for each experimental group/condition, given as a discrete number and unit of measurement
☐	☒	A statement on whether measurements were taken from distinct samples or whether the same sample was measured repeatedly
☐	☒	The statistical test(s) used AND whether they are one- or two-sided *Only common tests should be described solely by name; describe more complex techniques in the Methods section.*
☒	☐	A description of all covariates tested
☐	☒	A description of any assumptions or corrections, such as tests of normality and adjustment for multiple comparisons
☐	☒	A full description of the statistical parameters including central tendency (e.g. means) or other basic estimates (e.g. regression coefficient) AND variation (e.g. standard deviation) or associated estimates of uncertainty (e.g. confidence intervals)
☐	☒	For null hypothesis testing, the test statistic (e.g. *F*, *t*, *r*) with confidence intervals, effect sizes, degrees of freedom and *P* value noted *Give P values as exact values whenever suitable.*
☒	☐	For Bayesian analysis, information on the choice of priors and Markov chain Monte Carlo settings
☒	☐	For hierarchical and complex designs, identification of the appropriate level for tests and full reporting of outcomes
☐	☒	Estimates of effect sizes (e.g. Cohen's *d*, Pearson's *r*), indicating how they were calculated

Our web collection on statistics for biologists contains articles on many of the points above.

Software and code

Policy information about availability of computer code

Data collection	Windows Operating System version 10; Ubuntu Linux Operating System versions 16.04, 20.04; Python v2.6, v3.4, Neuralynx Cheetah and NetCom API V6.4; Robot Operating System (ROS) versions Kinetic, Noetic.
Data analysis	MATLAB versions 2021a, 2021b, 2022a; Various open-source third-party MATLAB packages from mathworks.org

For manuscripts utilizing custom algorithms or software that are central to the research but not yet described in published literature, software must be made available to editors and reviewers. We strongly encourage code deposition in a community repository (e.g. GitHub). See the Nature Portfolio guidelines for submitting code & software for further information.

Data

Policy information about availability of data

All manuscripts must include a data availability statement. This statement should provide the following information, where applicable:

- Accession codes, unique identifiers, or web links for publicly available datasets
- A description of any restrictions on data availability
- For clinical datasets or third party data, please ensure that the statement adheres to our policy

Preprocessed data used to perform the analyses and generate the figures in this manuscript are available in the Johns Hopkins Research Data Repository, at https://doi.org/10.7281/T1/THLC8N

Human research participants

Policy information about studies involving human research participants and Sex and Gender in Research.

Reporting on sex and gender	N/A
Population characteristics	N/A
Recruitment	N/A
Ethics oversight	N/A

Note that full information on the approval of the study protocol must also be provided in the manuscript.

Field-specific reporting

Please select the one below that is the best fit for your research. If you are not sure, read the appropriate sections before making your selection.

☒ Life sciences ☐ Behavioural & social sciences ☐ Ecological, evolutionary & environmental sciences

For a reference copy of the document with all sections, see nature.com/documents/nr-reporting-summary-flat.pdf

Life sciences study design

All studies must disclose on these points even when the disclosure is negative.

Sample size	No statistical methods were used to pre-determine sample size in these exploratory studies. The number of animals was determined based on standards used to established results in other peer-reviewed publications in the field (Jayakumar et al., 2019, Acharya et al., 2016, Purandare et al., 2022, Arleo et al., 2013, Pfeiffer and Foster, 2013). The number of sessions per animal varied based on behavioral state, number of units being recorded and observed stability of recordings.
Data exclusions	Sessions were excluded from analysis if they did not meet all of the following criteria. Criteria 1-4 are standard for our lab. Criterion 5 was specific for this experiment. (1) There were no experimental disruptions, such as too much manual intervention during the session or too many long breaks in recording due to behavioral performance or technical issues. (2) At least one unit deemed of cluster quality 4 or above, according to our manual quantification of cluster isolation quality. (3) At least one unit having more than 50 spikes during the session that fired when the animal ran at a velocity of more than 5 cm/s. (4) At least one unit classified as a putative pyramidal cell, using our classification based on mean firing rate, spike width, and typical ISI. (5). Sessions with stripe manipulation must have been run all the way to completion, i.e. the rat finished the session (Epoch 1-3, and removed after stripes were extinguished). Session inclusion was determined before performing any of the statistical analyses across sessions detailed in this manuscript.
Replication	We performed the experiment independently on five different individual rats, and all attempts at replication were successful. There have been no indications that would prevent future replication of these results, except the degradation of degree of control of the hippocampal place fields by optic flow, as observed in 1 of the 5 animals and in sessions categorized as "uncontrolled".
Randomization	There were no experimental groups for the subjects, since we ran similar open and closed loop sessions on 4 of the 5 animals used in this study. There were only open loop sessions collected from 1 of the 5 animals.
Blinding	The investigators were not blind to the identity of the animal or the experimental gain being applied during data collection. Blinding to the identity of the animal was impossible since animals underwent the experiment sequentially, each animal being tested over a few weeks. Gains were visible to the experimenters through the interface and could otherwise be easily deduced from viewing the movement of the projected image. Isolation and classification of clusters, however, was done blind to the experimental manipulation being applied. The data analysis software was also blind to the parameters of the trial.

Reporting for specific materials, systems and methods

We require information from authors about some types of materials, experimental systems and methods used in many studies. Here, indicate whether each material, system or method listed is relevant to your study. If you are not sure if a list item applies to your research, read the appropriate section before selecting a response.

Materials & experimental systems

n/a	Involved in the study
☒	☐ Antibodies
☒	☐ Eukaryotic cell lines
☒	☐ Palaeontology and archaeology
☐	☒ Animals and other organisms
☒	☐ Clinical data
☒	☐ Dual use research of concern

Methods

n/a	Involved in the study
☒	☐ ChIP-seq
☒	☐ Flow cytometry
☒	☐ MRI-based neuroimaging

Animals and other research organisms

Policy information about studies involving animals; ARRIVE guidelines recommended for reporting animal research, and Sex and Gender in Research

Laboratory animals	Rattus norvegicus, Long Evans, 3 Male and 2 Female, 5-8 months old, 300-450 g. weight
Wild animals	No wild animals were used in this study.
Reporting on sex	Sex wasn't considered in the study design. The findings apply to both sexes as the data are reported by rat as appropriate in the results and there were no obvious differences in results between male and female rats.
Field-collected samples	No field-collected samples were used in the study.
Ethics oversight	All animal care and housing procedures complied with National Institutes of Health guidelines and followed protocols approved by the Institutional Animal Care and Use Committee at Johns Hopkins University.

Note that full information on the approval of the study protocol must also be provided in the manuscript.